Check for updates

JGR Earth Surface

RESEARCH ARTICLE
10.1029/2023JF007217

Magnesium Isotope Variations in Granite Regoliths From Two Contrasting Climates

Ting Gao[1,2], Meng Qi[1,2], Zhengrong Wang[3], Runsheng Yin[1], Chengshuai Liu[1], Yuhui Liu[1,2], Shan Ke[4], and Zhi-Qi Zhao[5]

[1]State Key Laboratory of Environmental Geochemistry, Institute of Geochemistry, Chinese Academy of Sciences, Guiyang, China, [2]University of Chinese Academy of Sciences, Beijing, China, [3]Department of Earth & Atmospheric Sciences, The City College of New York, CUNY, New York, NY, USA, [4]State Key Laboratory of Geological Process and Mineral Resources, School of Earth Science and Resources, China University of Geosciences, Beijing, China, [5]School of Earth Science and Resources, Chang'an University, Xi'an, China

Key Points:

- Magnesium isotope fractionation differs significantly during granite weathering in temperate and tropical climate zones
- The formation of illite results in heavy magnesium isotope enrichment in solid weathering products
- Atmospheric deposition contributes a mass of light magnesium isotopes to shallow regolith under extremely weathered conditions

Supporting Information:

Supporting Information may be found in the online version of this article.

Correspondence to:

C. Liu,
liuchengshuai@vip.gyig.ac.cn

Citation:

Gao, T., Qi, M., Wang, Z., Yin, R., Liu, C., Liu, Y., et al. (2023). Magnesium isotope variations in granite regoliths from two contrasting climates. *Journal of Geophysical Research: Earth Surface*, *128*, e2023JF007217. https://doi.org/10.1029/2023JF007217

Received 24 APR 2023
Accepted 19 SEP 2023

Author Contributions:

Funding acquisition: Chengshuai Liu
Investigation: Ting Gao
Methodology: Ting Gao, Meng Qi, Yuhui Liu
Supervision: Chengshuai Liu
Writing – original draft: Ting Gao
Writing – review & editing: Ting Gao, Meng Qi, Zhengrong Wang, Runsheng Yin, Chengshuai Liu, Shan Ke, Zhi-Qi Zhao

© 2023. American Geophysical Union. All Rights Reserved.

Abstract Magnesium (Mg) isotopes have been utilized to constrain continental weathering; however, to date, little is known about the climate effects on Mg isotope fractionation during weathering. In this study, we measured δ^{26}Mg values of bulk regolith and exchangeable fraction in two granite regolith profiles developed under temperate, semiarid and tropical, humid climate conditions, respectively. Combined with mineralogy and element composition, we aimed to investigate how climate influences fractionation patterns of Mg isotopes during chemical weathering. At the temperate site, δ^{26}Mg values of regolith are slightly higher than that of the bedrock and negatively correlated with $\tau_{Mg,Th}$. Correspondingly, the exchangeable Mg is characterized by low δ^{26}Mg values. These results can be explained by the formation of small number of clay minerals. For the tropical regolith profile, δ^{26}Mg values decrease toward the surface, and the regolith has either lower δ^{26}Mg values above −250 cm or higher δ^{26}Mg values below −250 cm relative to the bedrock. The δ^{26}Mg value of exchangeable Mg is markedly lower than that of the regolith and varies significantly. These results can be explained by the mixing of Mg from solid weathering products and atmospheric deposition. The Mg from rainwater and/or marine aerosol deposit on the regolith and some may enter the crystal structure of the illite. The deposited Mg can overprint the granitic Mg, and the δ^{26}Mg value of shallow regolith samples will reflect mixing between granitic and atmospheric sources. The compilation of our and previously published Mg isotopic data reveals the potential control of climate on Mg isotope fractionation during continental weathering.

Plain Language Summary The isotopes of magnesium (Mg) can serve as a useful tracer in understanding the chemical weathering processes of silicate rocks. Previous studies have mainly focused on Mg isotope fractionation during silicate weathering by investigating single weathering profiles that have developed under constant climate conditions; however, the impact of climate on Mg isotope fractionation during silicate weathering remains poorly understood. Here, we analyzed Mg isotope compositions in two granite regolith profiles developed under temperate (semiarid) and tropical (humid) climate conditions. Our study suggests that the patterns of Mg mobilization and Mg isotope fractionation during granite weathering differ significantly in distinct climate zones. The compilation of our and previously published Mg isotopic data reveals that climate may have a huge impact on Mg isotope fractionation during terrestrial weathering, which is of significance to interpret the Mg isotope compositions of weathering products and river waters at a global scale.

1. Introduction

Carbon dioxide (CO_2) is a greenhouse gas, and the variation of atmospheric CO_2 level is an essential driving force for climate change on Earth (e.g., Berner et al., 1983; Brady, 1991; Murphy et al., 2016; Volk, 1987). The chemical weathering of silicate rocks provides metal ions (particularly Ca and Mg) that combine with dissolved CO_2 to form carbonates, which is one of the most important processes modulating Earth's climate (e.g., Berner et al., 1983; Dessert et al., 2003; Gaillardet et al., 1999). The variations of metal concentrations and their isotope compositions in regolith profiles can provide important insights into the mechanism of chemical weathering and the continental fluxes of metals to the ocean.

Magnesium (Mg) is a common constituent in silicate rocks. Weathering of silicate rocks releases large amounts of dissolved Mg^{2+} ions that are transported into the oceans by surface runoff. Fractionation of Mg isotopes (^{24}Mg, ^{25}Mg, and ^{26}Mg) can provide useful constraints on chemical weathering. Silicate rocks (e.g., ultramafic

21699011, 2023, 10, Downloaded from https://agupubs.onlinelibrary.wiley.com/doi/10.1029/2023JF007217 by CAS - Chengdu Library, Wiley Online Library on [16/04/2024]. See the Terms and Conditions (https://onlinelibrary.wiley.com/terms-and-conditions) on Wiley Online Library for rules of use; OA articles are governed by the applicable Creative Commons License

to felsic igneous rocks) usually have a narrow range of δ^{26}Mg values (−0.3‰ to −0.1‰) due to the limited Mg isotope fractionation during magmatic processes (Teng, Li, Ke, et al., 2010). In contrast, significant Mg isotope fractionation can occur during chemical weathering (e.g., Tipper et al., 2006; Wimpenny et al., 2010). For example, experimental studies have shown the preferential release of ^{24}Mg due to (a) kinetic effects during the dissolution of silicate minerals in early weathering stages (Maher et al., 2016; Wimpenny et al., 2010) and (b) the preferential dissolution of isotopically distinct mineral phases (Ryu et al., 2011). The largest Mg isotope fractionations are suggested to result from the incorporation of ^{26}Mg into structural sites of clay minerals (Wimpenny et al., 2014), consistent with most field studies showing the enrichment of ^{26}Mg in regolith samples (e.g., Bolou-Bi et al., 2012; Fan et al., 2023; Liu et al., 2014; Teng, Li, Rudnick, & Gardner, 2010; Tipper et al., 2012) and the enrichment of ^{24}Mg in waters (Bolou-Bi et al., 2012; Brenot et al., 2008; Pogge von Strandmann et al., 2008, 2012; Tipper et al., 2006, 2008, 2010, 2012; Wimpenny et al., 2011) relative to their bedrocks. Most of these studies emphasize a first-order control of ^{26}Mg enrichment in solid weathering products due to the formation of clay minerals.

The direction and extent of Mg isotope fractionation during the formation of various clay minerals are still debatable. However, they can be qualitatively explained by variations in the bond length of Mg–O in octahedral sites of clay minerals (Hindshaw et al., 2020). For example, smectite mineral phases (stevensite and saponite) and chrysotile show enrichment in ^{24}Mg compared with $Mg(H_2O)_6^{2+}$ dissolved in a coexisting solution (Hindshaw et al., 2020; Wimpenny et al., 2010), whereas kerolite and lizardite show the opposite pattern (Ryu et al., 2016; Wimpenny et al., 2014). Theoretical calculations predict that brucite preferentially incorporates ^{26}Mg compared with $Mg(H_2O)_6^{2+}$ (Colla et al., 2018; C. Gao et al., 2018; Wang et al., 2019), which is in accordance with experimental results at 80°C (Wimpenny et al., 2014), but in conflict with the experimental results at <50°C (Li et al., 2014). Light Mg isotopes have been suggested to be preferentially taken out from surfaces or interlayers of clay minerals during adsorption-desorption and cation exchange processes (Huang et al., 2012; Jacobson et al., 2010; Opfergelt et al., 2014), while recent studies have suggested that the Mg isotope composition of exchangeable Mg is identical to that of fluid phases (Cai et al., 2022; Wimpenny et al., 2014). The Mg isotope fractionation during the adsorption/incorporation of Mg onto/into (hydr)oxides remains unknown, but field observations suggested that the formation of crystalline Fe/Al-oxides may preferentially take up heavy Mg isotopes (Chapela Lara et al., 2017; T. Gao et al., 2018; Liu et al., 2014). Besides, repeated dissolution and precipitation of Fe oxides (Chapela Lara et al., 2017; T. Gao et al., 2018), phyllosilicate transformation (Li et al., 2021), progressive mineral transformations (Brewer et al., 2018; Ryu et al., 2021), transport of isotopically distinct fine particles (Ma et al., 2015), plant cycling (Bolou-Bi et al., 2012; Ryu et al., 2021; Schuessler et al., 2018; Uhlig et al., 2017), and atmospheric deposition (Chapela Lara et al., 2017; Liu et al., 2014; Opfergelt et al., 2012, 2014) could also shift the δ^{26}Mg values of weathering residues to be lower than those of their bedrock.

Early studies have indicated strong climatic control on chemical weathering (e.g., Berner et al., 1983; Brady, 1991; Murphy et al., 2016; Volk, 1987). Increased temperature and precipitation are thought to be key factors in accelerating the terrestrial chemical weathering (e.g., Brady, 1991; Hayes et al., 2020). Currently, however, the impact of climate on Mg isotope fractionation during chemical weathering remains poorly understood. Previous studies have mainly focused on how chemical weathering controls Mg isotope fractionation by investigating single weathering profiles that have experienced a constant climate during their development (e.g., Cai et al., 2022; Huang et al., 2012; Li et al., 2021; Liu et al., 2014; Opfergelt et al., 2012, 2014; Teng, Li, Rudnick, & Gardner, 2010), and few studies have paid attention to the linkage between Mg isotope fractionation and climatic parameters (e.g., Ryu et al., 2021). In this study, the mineralogy, element composition, and Mg isotope compositions of two granite regolith profiles (one from Beijing, China developed under a semiarid temperate climate and the other from Guangdong Province, China, developed under a humic tropical climate) were systematically investigated to understand the potential impact of climatic factors on Mg isotope fractionation during chemical weathering of granite. We also measured the Nd isotope ratios to estimate the potential impact of aeolian inputs on the Mg isotope composition of the regolith.

2. Site Description and Sample Collection

The two regolith profiles studied are developed on granitic rocks in Beijing (115° 56′ 40″E, 39° 42′ 36″N) and Guangdong (110° 20′ 17″E, 21° 27′ 35″N), which have temperate and tropical climates typical of North and South China, respectively (Figure 1). The physical and climatic characteristics of the regolith profiles are presented in Table S1 in Supporting Information S1.

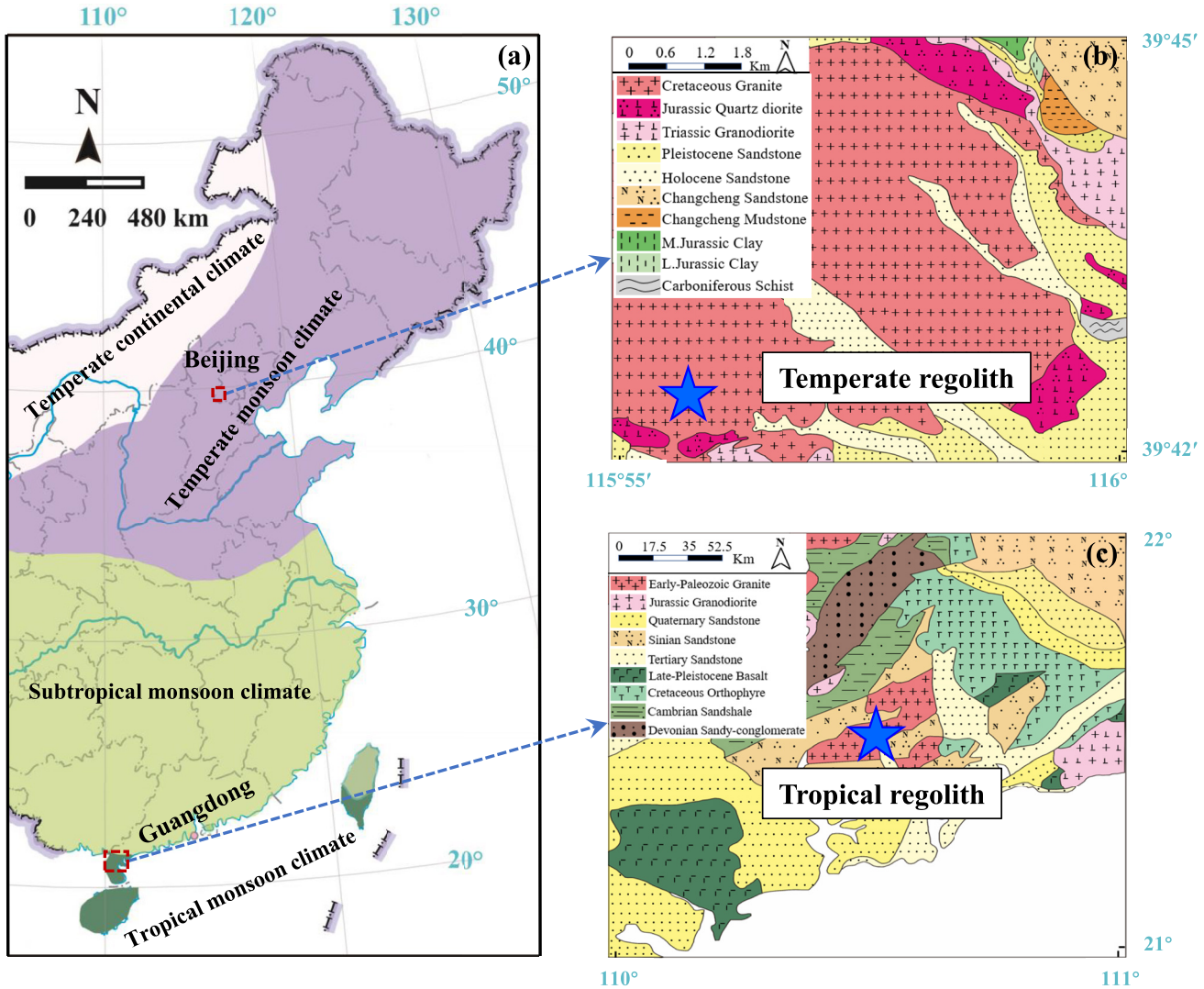

Figure 1. Map showing the geology, locations, and climatic characteristics of the two regolith profiles. The blue star represents the sampling site.

The regolith profile (BJ) close to Beijing (in North China) was sampled in a quarry on a ridge top. This region has a temperate, semiarid, and monsoonal climate. The mean annual temperature is ~12.2°C, with maximum monthly temperatures of 30–31°C during June and August, and minimum monthly temperatures of −9 to −6°C during December and February (http://data.cma.cn/). The mean annual precipitation is ~539 mm, with more than ~60% of the rainfall occurring from July to August. The bedrock is medium-grained granodiorite with plagioclase and K-feldspar megacrysts, which make up ~15 vol% of the total batholith. The studied granodiorite has a zircon U–Pb age of 130.7 ± 1.4 Ma (Cai et al., 2005) and contains quartz (12.4 wt%), plagioclase (67.6 wt%), K-feldspar (6.2 wt%), hornblende (8.3 wt%), and biotite (5.5 wt%) (Table S1 in Supporting Information S1). Hornblende and biotite occur as the dominant magnesian silicate phases in this granodiorite. The regolith profile is ~240 cm deep and shows an undisturbed progression of weathering intensity toward the surface. Nine regolith samples were collected from the profile. The regolith sample above ~80 cm is loose saprolite, which was sampled at an interval of ~10 cm by dredging. Below ~80 cm, saprocks are dense, and were sampled where drilling was feasible. Unaltered granodioritic bedrock was sampled at the bottom of the regolith profile. The vegetation cover is sparse and mainly consists of small annual herbaceous plants. The topsoil above ~40 cm with visible roots was not sampled to minimize anthropogenic and biological effects.

The tropical regolith profile (GD) was sampled at a roadcut on a ridge top about 70 km away from the coast in the southwestern part of Guangdong Province, South China. This area is characterized by a tropical, humid, and

21699011, 2023, 10, Downloaded from https://agupubs.onlinelibrary.wiley.com/doi/10.1029/2023JF007217 by CAS - Chengdu Library, Wiley Online Library on [16/04/2024]. See the Terms and Conditions (https://onlinelibrary.wiley.com/terms-and-conditions) on Wiley Online Library for rules of use; OA articles are governed by the applicable Creative Commons License

monsoonal climate. The mean annual temperature is ~23.5°C, with maximum monthly temperatures of 30–32°C during July and August, and minimum monthly temperatures of 5–20°C during January and February (http://data.cma.cn/). The mean annual precipitation is ~1,691 mm, with over ~80% of the rainfall occurring during the warm season from May to October. The bedrock is medium-grained granite with plagioclase megacrysts. The bedrock at this site was formed in the Jurassic with a zircon U–Pb age of 150–180 Ma (Li et al., 2007). It mainly contains quartz (37.5 wt%), plagioclase (56.0 wt%), and biotite (6.5 wt%) (Table S1 in Supporting Information S1). Biotite is the dominant Mg-bearing silicate phase in the studied granite. The regolith profile is ~710 cm deep and has a sharp transition from unweathered rock to highly weathered regolith. Thirty-five regolith samples were collected at an interval of ~20 cm. Unaltered bedrock was sampled from a nearby outcrop. The vegetation cover is dense and mainly consists of small annual eucalyptus plants. The topsoil above ~30 cm with visible roots was not sampled to minimize the effect of anthropogenic and biological activities.

The regolith samples were air-dried, crushed into fine powder (~30 g) using an agate mortar, and passed through a 200-mesh (0.075 mm) nylon sieve, prior to chemical analyses. Given the potentially different responses to weathering between hornblende and biotite minerals for the temperate profile, these two types of minerals were separated to analyze Mg isotope compositions. Granodiorite was first crushed into 40–80 mesh (0.177–0.42 mm), and hornblende and biotite minerals were then picked under a binocular microscope. Both mineral fractions were unaltered and approximately 100% pure after handpicking twice.

3. Analytical Methods

3.1. Determination of the Total Organic Carbon (TOC) Content

The TOC content of the regolith samples was determined using an elemental analyzer (Elementar vario MACRO cube, Germany) at the Institute of Geochemistry, Chinese Academy of Sciences (IGCAS). Prior to measurements, the samples were treated with 2 mol L^{-1} HCl until complete carbonate removal and heated for 3 hr at 75°C. The analytical precision for TOC was better than 0.5%.

3.2. Identification and Quantification of Mineral Phases

Mineral phases and modes were determined by an X-ray diffractometer (Bruker D2, Germany) at the Institute of Eco-environmental and Soil Sciences, Guangdong Academy of Sciences, China. The bulk samples were ground into fine powders (<300 mesh). All analyses were performed using a Si low background sample holder. The X-ray scanning range was 5–85° with a scanning speed of 1.2°/min, and the step size was 0.02° with Co/Kα radiation. Quantitative analysis of the mineral mode was conducted using the Rietveld method (R. A. Young, 1993) and the TOPAS V5 program (Bruker AXS, Germany), with uncertainties determined by the variance of the least squared fit. The mineral structure files were downloaded from the COD (Crystallography Open Database) database (Graulis et al., 2009), and the Rwp (R-weighted pattern) values of all fittings were lower than 12.0 to ensure good fitting quality.

To determine the secondary clay minerals in the temperate regolith samples, we conducted elemental mapping (~30 × 20 μm) using a scanning electron microscope (SEM, Scios, Thermo Fisher Scientific Inc, USA) equipped with an energy dispersive spectroscopy detector (EDS, Thermo Fisher Scientific Inc, USA) at IGCAS. SEM and EDS elemental mapping was operated at 15 kV with a 1.6 nA electric current. The working distance of the detector to the sample was 5.6 mm for SEM. The takeoff angle, live time, amp time, and energy resolution of EDS were 33.5°, 8.8 s, 0.45 μs, and 130.7 eV, respectively.

3.3. Major and Trace Element Analyses

Major element analyses were performed at Guizhou Tongwei Analytical Technology Co., Ltd., China, using an X-ray fluorescence spectrometer (XRF, PANalytical Axios PW4400, Netherlands). Replicate measurements of GSP-2, a geological standard reference material (granite), yielded a relative difference <±1% compared with the certified value.

Trace elements were determined via inductively coupled plasma mass spectrometry (ICP-MS, PerkinElmer® NexION 300X, USA) at Guizhou Tongwei Analytical Technology Co., Ltd., China. Prior to analysis, ~40 mg of

21699011, 2023, 10, Downloaded from https://agupubs.onlinelibrary.wiley.com/doi/10.1029/2023JF007217 by CAS - Chengdu Library, Wiley Online Library on [16/04/2024]. See the Terms and Conditions (https://onlinelibrary.wiley.com/terms-and-conditions) on Wiley Online Library for rules of use; OA articles are governed by the applicable Creative Commons License

21699011, 2023, 10, Downloaded from https://agupubs.onlinelibrary.wiley.com/doi/10.1029/2023JF007217 by CAS - Chengdu Library, Wiley Online Library on [16/04/2024]. See the Terms and Conditions (https://onlinelibrary.wiley.com/terms-and-conditions) on Wiley Online Library for rules of use; OA articles are governed by the applicable Creative Commons License

sample powder was completely digested in ~3.5 mL of a 1:1:3 mixture of HF-HCl-HNO_3 in high-pressure Parr digestion vessels. The internal standard Rh was used to control instrumental drift, and GSP-2 was used for quality control. Repetitive measurements of GSP-2 yielded a relative uncertainty of less than ±5% for the elements reported.

3.4. Sequential Extraction Experiment

Sequential extraction was conducted to separate the four operationally defined Mg fractions from bulk samples (Bolou-Bi et al., 2012; Wiederhold et al., 2007), including (a) the exchangeable fraction (e.g., Mg in interlayers and surfaces of clays and Fe/Mn oxides; using 1 mol L^{-1} NH_4-acetate, pH = 7), (b) amorphous minerals (e.g., Mg in ferrihydrite; using 0.5 mol L^{-1} HCl), (c) crystalline Fe-oxides (e.g., Mg in goethite and hematite; using 1 mol L^{-1} NH_2OH-HCl), and (d) silicate residuals (e.g., Mg in primary minerals and structures of clays). The details of the sequential extraction procedure are provided in Table S2 in Supporting Information S1. During the first three steps, each supernatant solution was separated from the insoluble residue by centrifugation at ~8,400 × g for 8 min. The Mg concentrations of these solutions were measured by atomic absorption spectrometry (AAS, PerkinElmer® PinAAcle 900F, USA) at IGCAS. Due to the low concentration of Mg in the silicate residue, which accounts for only a small fraction of the total Mg budget in these samples, the Mg content in silicate residues was not measured directly but calculated by subtracting the sum of the extracted solutions from the total concentration.

3.5. Mg Isotope Analysis

Magnesium isotope ratios were determined for bulk regolith samples and the exchangeable fractions obtained by sequential extraction in this study. The purification of Mg was conducted in class-1000 clean laboratory room either at IGCAS or at the China University of Geosciences (CUGB). The utilized acids including HF, HCl, and HNO_3 were guaranteed reagents and further purified by the sub-boiling distillation system (Savillex DST-1000, USA). Ultrapure water (18.2 MΩ·cm^{-1}) was obtained using a Milli-Q® Element system (Millipore Reference A+, USA). H_2O_2 (trace analysis grade) was purchased from Thermo Scientific™ (USA). Based on the Mg concentration, approximately 3–40 mg of powdered bulk sample material was dissolved in Teflon beakers in a 3:1 mixture of concentrated HF-HNO_3 and subsequently heated at 160°C for 2 d. After cooling, 1 mL of H_2O_2 (trace analysis grade) was added and then placed on a hot plate at 70°C for 1 hr to remove organic matter. Afterward, the sample solutions were dried and treated with a 3:1 mixture of HCl-HNO_3 to achieve complete digestion, followed by heating at 160°C for 2 d and then drying at 80°C. The samples were refluxed with concentrated HNO_3 at 140°C until complete dissolution was achieved and subsequently evaporated to complete dryness at 80°C. This dried residue was finally dissolved in 1 M HNO_3 in preparation for ion exchange column chemistry. The exchangeable fraction was treated with H_2O_2 and a mixture of HF-HNO_3-HCl, followed by dissolving in 1 M HNO_3 before chromatographic separation.

The separation of Mg was achieved by cation exchange chromatography by using AG50W-X8 resin (Bio-Rad 200–400 mesh, ~2.3 mL) following the method of Gao et al. (2019). Matrix elements were removed using 23 mL of 1 M HNO_3, and then Mg was eluted by 15 mL of 1 M HNO_3. The geological reference materials BHVO-2, BCR-2, and GSP-2 were processed together with samples for each purification session. The same column procedure was repeated twice to obtain a pure Mg solution for mass spectrometry. The total procedural blank was <10 ng, which represented <1‰ of the total Mg that was loaded on the column.

The Mg isotope ratios of all samples were analyzed at IGCAS or CUGB using a Neptune Plus multi-collector inductively coupled plasma mass spectrometer (MC-ICP-MS, Thermo Finnigan, Germany). The analysis was performed in a wet plasma mode and using the standard-sample bracketing technique. The GSB Mg solution (a pure Mg solution from the China Iron and Steel Research Institute) was used as an in-house standard. Each sample was measured at least two times to assess the precision of the measurements. The Mg isotope ratios of samples are reported as deviations from the DSM3 standard using the following equation:

$$\delta^{x}\mathrm{Mg} = \left[\frac{(^{x}\mathrm{Mg}/^{24}\mathrm{Mg})_{\mathrm{sample}}}{(^{x}\mathrm{Mg}/^{24}\mathrm{Mg})_{\mathrm{DSM3}}} - 1\right] \times 1000, \quad (1)$$

where x refers to a mass of 25 or 26. Two standard deviations (2SD) were reported throughout this paper. The δ^{25}Mg and δ^{26}Mg values of the GSB Mg standard relative to the DSM3 standard are −1.044 ± 0.024‰ and −2.032 ± 0.038‰ (2SD, n = 225), respectively, based on 4-year measurements in the CUGB lab (Gao et al., 2019).

21699011, 2023, 10, Downloaded from https://agupubs.onlinelibrary.wiley.com/doi/10.1029/2023JF007217 by CAS - Chengdu Library, Wiley Online Library on [16/04/2024]. See the Terms and Conditions (https://onlinelibrary.wiley.com/terms-and-conditions) on Wiley Online Library for rules of use; OA articles are governed by the applicable Creative Commons License

The USGS standards BHVO-2, BCR-2, and GSP-2 were analyzed along with the studied samples and yielded average δ^{26}Mg values of $-0.27 \pm 0.04‰$ (2SD, $n = 3$), $-0.17 \pm 0.07‰$ (2SD, $n = 3$), and $0.06 \pm 0.01‰$ (2SD, $n = 3$), respectively, which are consistent with previous studies (e.g., Teng et al., 2015).

3.6. Nd Isotope Analysis

The Nd isotope ratios were analyzed for some tropical regolith samples at Guizhou Tongwei Analytical Technology Co., Ltd., China. The digestion procedure was the same as that used for Mg isotope analysis. The Nd fraction was purified by cation exchange chromatography using TRU-spec resin and Ln-spec resin. Detailed procedures have been published in Wei et al. (2022). Purified sample solutions were analyzed for Nd isotopes using an MC-ICP-MS (Nu Plasma III, UK) and the instrumental mass bias was corrected using $^{146}Nd/^{144}Nd$ of 0.7219. Repeated analyses of JNdi (a Nd oxide from the Geological Survey of Japan with the a $^{143}Nd/^{144}Nd$ of 1.000503 ± 0.000001 relative to the LaJolla Nd isotope standard) give an average $^{143}Nd/^{144}Nd$ of 0.512112 ± 0.000010 (2SD; $n = 10$), which is consistent with the reference value of 0.512115 ± 0.000007 reported in Tanaka et al. (2000). The USGS standard BCR-2 yielded a $^{143}Nd/^{144}Nd$ of 0.512633 ± 0.000004 (2SD, internal precision), which is comparable to the recommended value (e.g., Jweda et al., 2016; Raczek et al., 2003). The isotopic value is reported as ε_{Nd}:

$$\varepsilon_{Nd} = \left[\frac{(^{143}Nd/^{144}Nd)_{measured}}{(^{143}Nd/^{144}Nd)_{CHUR}} - 1\right] \times 10000, \quad (2)$$

in which the $^{143}Nd/^{144}Nd$ of CHUR (chondritic uniform reservoir) is 0.512638.

3.7. Calculations of Mg Gain or Loss and Weathering Intensity

The gains and losses of Mg in regolith were defined as the percentage change in the concentration ratio of the element over a conservative element in a sample relative to that in the bedrock (Brimhall & Dietrich, 1987):

$$\tau_{Mg,X} = \left[\frac{C_{Mg,w}/C_{j,w}}{C_{Mg,p}/C_{j,p}} - 1\right] \times 100, \quad (3)$$

where X refers to a conservative element, $C_{Mg,w}$ and $C_{Mg,p}$ are concentrations of Mg in regolith samples (w) and their bedrock (p), respectively, and $C_{j,w}$ and $C_{j,p}$ are concentrations of the relatively conservative element (j) in regolith (w) and their bedrock (p), respectively. Positive (negative) $\tau_{Mg,X}$ values indicate enrichment (depletion) of Mg in the weathering profile relative to the bedrock. Elements such as Th, Zr, Ti, Ta, and Nb are suggested to be immobile during weathering (e.g., Braun et al., 1993; Kurtz et al., 2000; Nesbitt & Markovics, 1997; Nesbitt & Wilson, 1992). Our results show that percentage changes in Ti/Th, Nb/Th, Ta/Th, and Zr/Th ratios relative to the bedrock are all negative in temperate regolith samples (Table S3 in Supporting Information S1), suggesting that Th is the most immobile of these elements in this regolith. In contrast, Ta was evaluated to be the most conservative of these elements in tropical regolith samples.

The Chemical Index of Alteration (CIA) is commonly used to evaluate the intensity of chemical weathering (Nesbitt & Young, 1982):

$$CIA = \frac{Al_2O_3}{Al_2O_3 + CaO^* + Na_2O + K_2O} \times 100, \quad (4)$$

where CaO* refers to the total amount of Ca in minerals other than carbonate and phosphate.

4. Results

4.1. Mineral Compositions

The temperate regolith samples dominantly contain primary minerals, including hornblende (4.1–13.9 wt%), plagioclase (49.5–76.9 wt%), and K-feldspar (7.0–16.5 wt%), while biotite and secondary minerals are not identified using XRD (Table S4 in Supporting Information S1 and Figure 2). In contrast, the tropical regolith samples are dominated by secondary minerals, including kaolinite (32.8–52.9 wt%), illite (0–25.6 wt%), goethite (6.8–14.8 wt%), and hematite (1.7–6.9 wt%), with limited number of primary mineral phases.

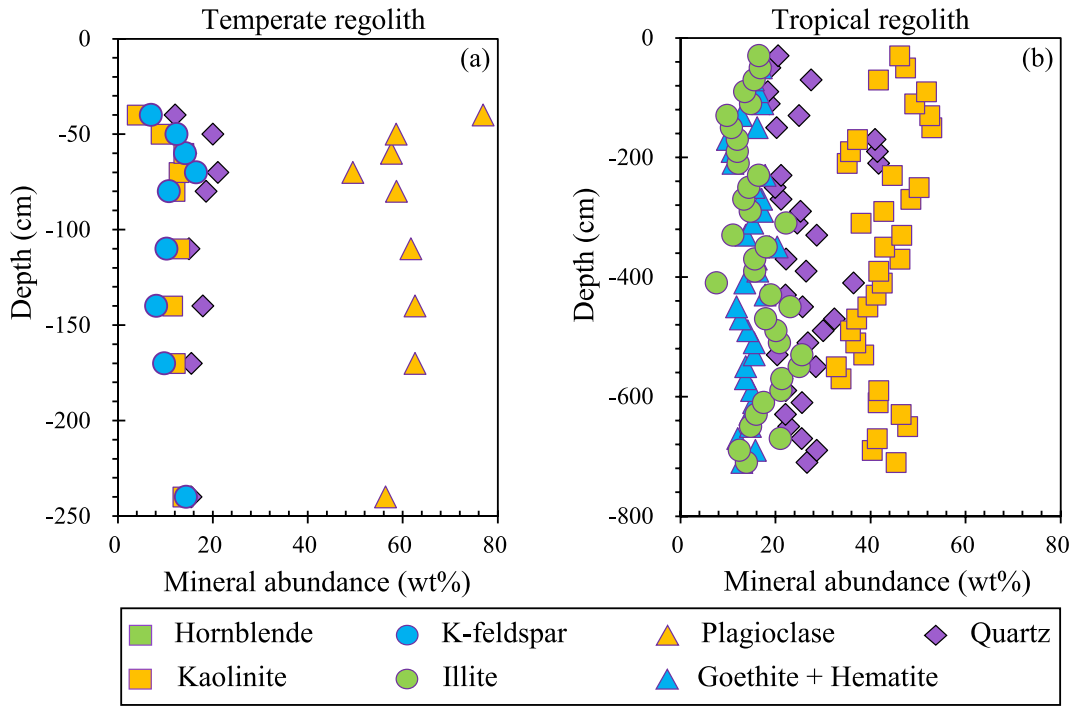

Figure 2. Mineral content versus depth in the temperate (a) and tropical (b) regolith profiles. Note that the *y*-axis in panel (b) has a different scale from that in panel (a).

4.2. Mg Contents and Fractions

The temperate regolith samples exhibited relatively limited variations in MgO concentrations (2.13%–3.18%), which were close to those of bedrock (2.55%) (Table S5 in Supporting Information S1 and Figure 3a). The $\tau_{Mg,Th}$ values vary from −51.2% to −7.9% and generally become more negative toward the surface (Table S5 in Supporting Information S1 and Figure 3b). In comparison, the tropical regolith samples have a much lower MgO concentration (0.18%–0.51%) than bedrock (1.54%) and show a more negative $\tau_{Mg,Ta}$ value (−82.3% to −93.8%). In both regolith profiles, residual silicates are the main Mg-bearing phases, accounting for 95%–98% of the total Mg in the temperate regolith and 92%–99% in the tropical regolith (Table S6 in Supporting Information S1 and Figures 3c and 3d). The fractions of Mg in the exchangeable pool (temperate: 0.77%–1.23%; tropical: 0.5%–3.67%), amorphous minerals (temperate: 0.88%–1.31%; tropical: 0.04%–0.72%), and crystalline Fe-oxides (temperate: 1.15%–1.71%; tropical: 0.50%–3.01%) were relatively small.

4.3. Mg Isotope Compositions

The granite bedrocks in the temperate and tropical regoliths have a mantle-like Mg isotope signature (−0.25 ± 0.07‰, 2SD, n = 139; Teng, Li, Ke, et al., 2010), with δ^{26}Mg values of −0.34‰ (n = 1) and −0.24‰ (n = 1), respectively (Table 1 and Figure 4). In the temperate regolith profile, the hornblende and biotite minerals separate from the unweathered granite have δ^{26}Mg values of −0.31 ± 0.05‰ (2SD, n = 2) and −0.26 ± 0.05‰ (2SD, n = 2), respectively, which are close to those of bulk bedrock. The regolith samples show slightly higher δ^{26}Mg values with increasing values of −0.32‰ at the bottom to −0.16‰ at the top. In contrast, at the tropical site, the δ^{26}Mg values of regolith samples cover a wide range from −0.54 to 0.21‰ (−0.16 ± 0.38‰, 2SD, n = 35) and decrease from the bottom to the top. Compared with its bedrock, the regolith is depleted in heavy Mg isotopes above a depth of approximately −250 cm (−0.39 ± 0.23‰, 2SD, n = 11), below which it is enriched in heavy Mg isotopes (−0.06 ± 0.21‰, 2SD, n = 24).

For most samples, the exchangeable Mg has a δ^{26}Mg value that is more negative than that of the bulk samples (Table 1 and Figure 4). The exchangeable Mg in the temperate regolith samples has a narrow range of δ^{26}Mg values between −0.45‰ and −0.53‰ (averaging −0.50 ± 0.05‰, 2SD, n = 8). In comparison, the exchangeable Mg

21699011, 2023, 10, Downloaded from https://agupubs.onlinelibrary.wiley.com/doi/10.1029/2023JF007217 by CAS - Chengdu Library, Wiley Online Library on [16/04/2024]. See the Terms and Conditions (https://onlinelibrary.wiley.com/terms-and-conditions) on Wiley Online Library for rules of use; OA articles are governed by the applicable Creative Commons License

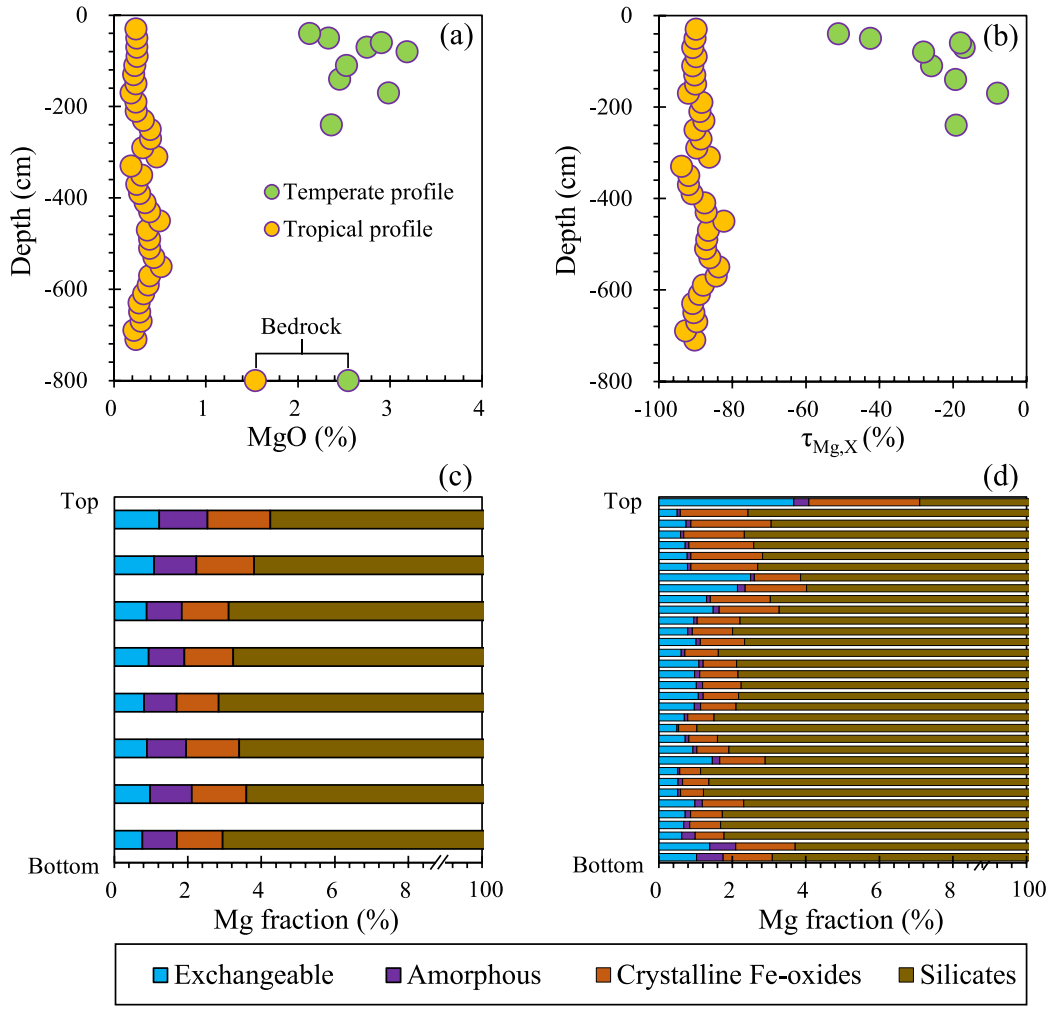

Figure 3. Bulk MgO content (a) and $\tau_{Mg,X}$ (b) versus depth, and the relative proportions of Mg in regolith extractions relative to the bulk in the temperate (c) and tropical (d) profiles. In plot (b), *X* refers to Th in the temperate regolith and Ta in the tropical regolith (see explanation in Section 3.7). Note that the *y*-axes in panels (b and d) have different scales from those in panels (a and c).

of regolith samples from the tropical profile exhibits δ^{26}Mg with a wide range (−1.30‰ to −0.39‰; averaging −0.66 ± 0.37‰, 2SD, n = 34). Significant δ^{26}Mg variations (−1.30‰ to −0.48‰; averaging −0.77 ± 0.51‰, 2SD, n = 11) were observed in the exchangeable pool of the regolith above −250 cm.

4.4. Nd Isotope Ratios

The tropical regolith samples have ε_{Nd} values ranging from −16.51 to −14.54 (Table S7 in Supporting Information S1). The regolith samples (−15.62 to −14.54) above a depth of approximately −250 cm have slightly higher ε_{Nd} values than the deep regolith samples (−16.15 to −15.61).

5. Discussion

The patterns of mobilization and isotope compositions of Mg in the two studied regoliths display significant differences (Figures 3 and 4), reflecting isotope fractionation regulated using different geochemical processes at distinct weathering stages. In the temperate site, regolith samples display Mg depletion and slightly higher δ^{26}Mg relative to the bedrock (Figure 4a), which mainly reflects the formation of small number of clay minerals at the incipient weathering stage. In contrast, in the tropical site, regolith displays significant Mg loss, and isotopically

21699011, 2023, 10, Downloaded from https://agupubs.onlinelibrary.wiley.com/doi/10.1029/2023JF007217 by CAS - Chengdu Library, Wiley Online Library on [16/04/2024]. See the Terms and Conditions (https://onlinelibrary.wiley.com/terms-and-conditions) on Wiley Online Library for rules of use; OA articles are governed by the applicable Creative Commons License

Table 1
Mg Isotope Compositions in Bedrock, Mineral Separates, Bulk Regolith, Exchangeable Pool, and Standards Analyzed for This Study

		Bulk regolith						Exchangeable pool					
Sample ID	Depth (cm)	δ^{25}Mg (‰)	2SD (‰)	δ^{26}Mg (‰)	2SD (‰)	Δ^{25}Mg′ (‰)	*n*	δ^{25}Mg (‰)	2SD (‰)	δ^{26}Mg (‰)	2SD (‰)	Δ^{25}Mg′ (‰)	*n*
Temperate regolith													
ZKD2-P	Bedrock	−0.17	0.06	−0.34	0.02	0.01	4	n.a.	n.a.	n.a.	n.a.	n.a.	n.a.
ZKD2-1	−240	−0.16	0.03	−0.32	0.02	0.01	4	n.a.	n.a.	n.a.	n.a.	n.a.	n.a.
ZKD2-2	−170	−0.14	0.04	−0.27	0.01	0.00	4	−0.28	0.05	−0.51	0.03	−0.01	3
ZKD2-3	−140	−0.14	0.02	−0.28	0.04	0.01	4	−0.28	0.01	−0.53	0.03	0.00	2
ZKD2-4	−110	−0.12	0.01	−0.24	0.04	0.01	4	−0.25	0.01	−0.50	0.02	0.01	2
ZKD2-5	−80	−0.12	0.04	−0.24	0.01	0.01	4	−0.27	0.03	−0.50	0.02	−0.01	2
ZKD2-6	−70	−0.10	0.04	−0.20	0.02	0.01	4	−0.26	0.02	−0.50	0.02	−0.01	2
ZKD2-7	−60	−0.11	0.05	−0.22	0.01	0.00	4	−0.24	0.02	−0.52	0.01	0.03	2
ZKD2-8	−50	−0.11	0.01	−0.21	0.03	0.00	4	−0.25	0.00	−0.45	0.03	−0.02	2
ZKD2-9	−40	−0.08	0.02	−0.17	0.02	0.01	4	−0.26	0.08	−0.50	0.06	0.00	2
Hornblende (1)		−0.11	0.02	−0.28	0.03	0.04	4						
Hornblende (2)		−0.14	0.07	−0.33	0.06	0.03	4						
Biotite (1)		−0.11	0.03	−0.28	0.03	0.04	4						
Biotite (2)		−0.12	0.03	−0.23	0.03	0.00	4						
Tropical regolith													
ZJ2-P	Bedrock	−0.12	0.04	−0.24	0.04	0.00	2						
ZJ2-1	−710	0.06	0.02	0.12	0.02	0.00	3	−0.33	0.04	−0.64	0.05	0.01	3
ZJ2-2	−690	0.11	0.05	0.21	0.07	0.01	3	−0.22	0.06	−0.47	0.08	0.02	3
ZJ2-3	−670	−0.01	0.07	−0.03	0.07	0.01	3	−0.41	0.05	−0.79	0.06	0.01	3
ZJ2-4	−650	−0.04	0.04	−0.10	0.02	0.00	3	−0.27	0.09	−0.52	0.08	0.00	3
ZJ2-5	−630	−0.09	0.02	−0.17	0.00	0.00	2	−0.42	0.04	−0.81	0.05	0.00	3
ZJ2-6	−610	−0.06	0.02	−0.10	0.08	0.01	2	−0.22	0.01	−0.39	0.07	−0.01	3
ZJ2-7	−590	−0.01	0.00	−0.04	0.05	0.00	2	−0.29	0.06	−0.61	0.04	0.03	3
ZJ2-8	−570	0.01	0.02	0.01	0.05	0.01	2	−0.29	0.06	−0.58	0.05	0.01	3
ZJ2-9	−550	0.08	0.01	0.14	0.00	0.01	2	n.a.	n.a.	n.a.	n.a.	n.a.	n.a.
ZJ2-10	−530	−0.02	0.06	−0.03	0.04	0.00	2	−0.36	0.03	−0.64	0.04	−0.03	3
ZJ2-11	−510	−0.02	0.02	−0.09	0.04	0.02	2	−0.31	0.05	−0.62	0.06	0.02	3
ZJ2-12	−490	−0.05	0.03	−0.09	0.04	0.00	5	−0.31	0.07	−0.56	0.04	−0.01	3
ZJ2-13	−470	−0.05	0.06	−0.11	0.04	0.01	4	−0.26	0.05	−0.49	0.06	0.00	3
ZJ2-14	−450	0.03	0.04	0.04	0.03	0.01	4	−0.27	0.06	−0.55	0.04	0.02	3
ZJ2-15	−430	−0.02	0.04	−0.03	0.09	0.00	2	−0.31	0.09	−0.61	0.02	0.01	3
ZJ2-16	−410	−0.04	0.03	−0.08	0.05	0.00	3	−0.26	0.04	−0.52	0.02	0.01	3
ZJ2-17	−390	−0.01	0.01	−0.06	0.05	0.02	2	−0.41	0.01	−0.80	0.00	0.00	3
ZJ2-18	−370	−0.10	0.03	−0.20	0.07	0.00	3	−0.28	0.03	−0.57	0.02	0.01	3
ZJ2-19	−350	−0.03	0.01	−0.02	0.02	−0.02	3	−0.25	0.02	−0.52	0.01	0.02	4
ZJ2-20	−330	−0.11	0.02	−0.21	0.07	0.00	3	−0.35	0.03	−0.67	0.06	0.00	3
ZJ2-21	−310	−0.06	0.08	−0.09	0.05	−0.01	2	−0.29	0.03	−0.56	0.03	0.00	3
ZJ2-22	−290	−0.10	0.01	−0.20	0.05	0.00	3	−0.38	0.02	−0.78	0.01	0.02	3
ZJ2-23	−270	−0.10	0.04	−0.19	0.06	−0.01	3	−0.32	0.04	−0.64	0.00	0.02	3
ZJ2-24	−250	−0.05	0.06	−0.09	0.04	0.00	3	−0.33	0.03	−0.70	0.03	0.03	3

21699011, 2023, 10, Downloaded from https://agupubs.onlinelibrary.wiley.com/doi/10.1029/2023JF007217 by CAS - Chengdu Library, Wiley Online Library on [16/04/2024]. See the Terms and Conditions (https://onlinelibrary.wiley.com/terms-and-conditions) on Wiley Online Library for rules of use; OA articles are governed by the applicable Creative Commons License

Table 1
Continued

Sample ID	Depth (cm)	Bulk regolith δ^{25}Mg (‰)	2SD (‰)	δ^{26}Mg (‰)	2SD (‰)	Δ^{25}Mg′ (‰)	*n*	Exchangeable pool δ^{25}Mg (‰)	2SD (‰)	δ^{26}Mg (‰)	2SD (‰)	Δ^{25}Mg′ (‰)	*n*
ZJ2-25	−230	−0.14	0.03	−0.29	0.05	0.01	3	−0.47	0.00	−0.86	0.01	−0.02	3
ZJ2-26	−210	−0.23	0.01	−0.44	0.05	0.00	3	−0.49	0.03	−0.93	0.02	−0.01	3
ZJ2-27	−190	−0.08	0.06	−0.14	0.05	0.00	2	−0.58	0.04	−1.13	0.01	0.01	3
ZJ2-28	−170	−0.26	0.01	−0.50	0.03	0.00	2	−0.69	0.03	−1.30	0.06	−0.01	3
ZJ2-29	−150	−0.13	0.03	−0.28	0.07	0.01	2	−0.38	0.08	−0.71	0.06	−0.01	3
ZJ2-30	−130	−0.24	0.06	−0.50	0.09	0.01	2	−0.24	0.03	−0.48	0.07	0.01	3
ZJ2-31	−110	−0.20	0.00	−0.40	0.02	0.01	2	−0.25	0.02	−0.50	0.02	0.01	3
ZJ2-32	−90	−0.28	0.03	−0.54	0.06	0.00	3	−0.26	0.02	−0.50	0.05	0.00	3
ZJ2-33	−70	−0.24	0.06	−0.49	0.08	0.02	2	−0.31	0.10	−0.61	0.06	0.01	3
ZJ2-34	−50	−0.21	0.02	−0.39	0.06	0.00	2	−0.33	0.03	−0.70	0.07	0.04	3
ZJ2-35	−30	−0.18	0.04	−0.35	0.04	0.01	2	−0.41	0.05	−0.79	0.05	0.00	3
Reference materials													
BHVO-2		−0.14	0.05	−0.27	0.04	0.00	3						
BCR-2		−0.08	0.05	−0.17	0.07	0.01	3						
GSP-2		0.04	0.01	0.06	0.01	0.01	3						

Note. 2SD = two times the standard deviations; *n* = number of measurements by MC-ICP-MS. Δ^{25}Mg' is the deviation from the predicted equilibrium mass-dependent fractionation law (slope = 0.521; E. D. Young and Galy, 2004). n.a. = not analyzed. The Mg isotope ratios of bulk regolith samples at the temperate site were analyzed at CUGB and those of other samples were analyzed at IGCAS.

heavy Mg is either enriched in the deep regolith (below −250 cm) or depleted in the shallow regolith (above −250 cm) (Figure 4b). This is likely a result of a combination of clay mineral formation and atmospheric deposition from marine aerosols and/or rainwater under extreme weathering conditions. Below, we will discuss these processes in detail.

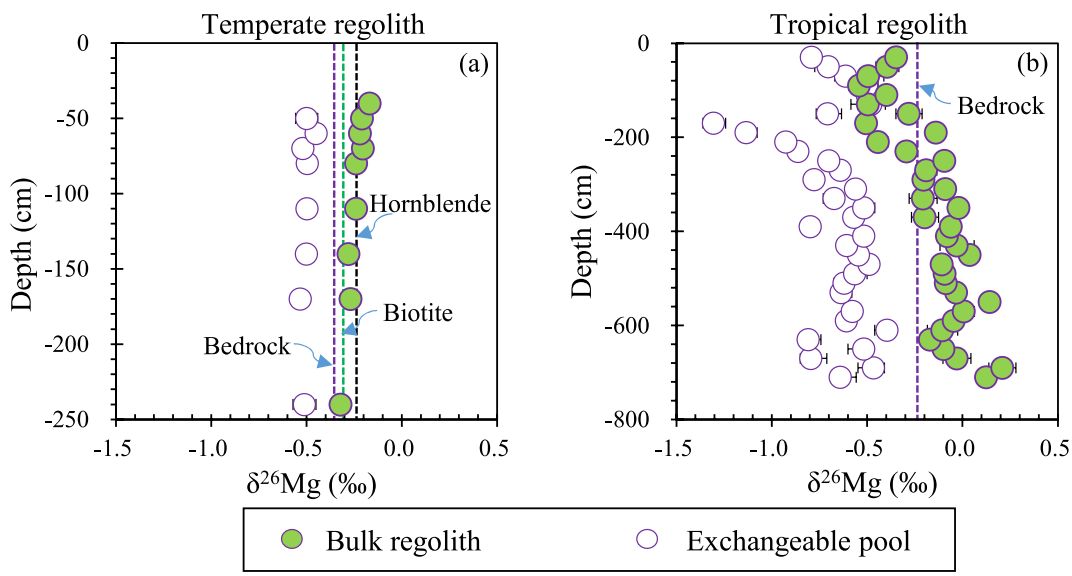

Figure 4. The δ^{26}Mg values of exchangeable and bulk Mg versus depth in the temperate (a) and tropical (b) regolith profiles. The δ^{26}Mg values of bedrock, biotite, and hornblende are shown as purple, green, and black dotted lines, respectively. Error bars represent 2SD uncertainties. Note that the *y*-axis in panel (b) has a different scale from that in panel (a).

21699011, 2023, 10, Downloaded from https://agupubs.onlinelibrary.wiley.com/doi/10.1029/2023JF007217 by CAS - Chengdu Library, Wiley Online Library on [16/04/2024]. See the Terms and Conditions (https://onlinelibrary.wiley.com/terms-and-conditions) on Wiley Online Library for rules of use; OA articles are governed by the applicable Creative Commons License

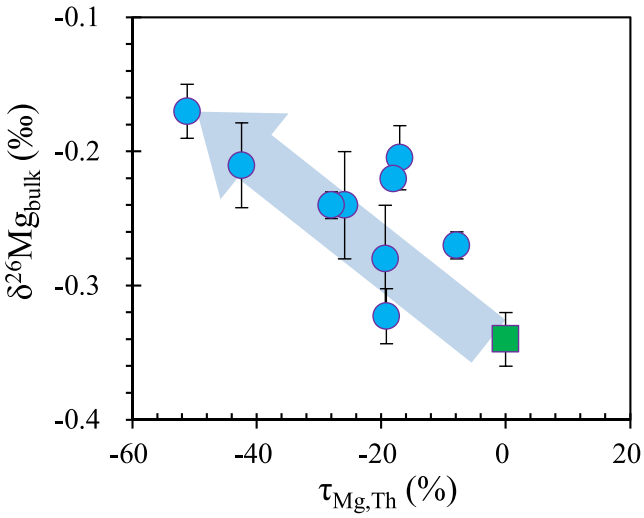

Figure 5. $\tau_{Mg,Th}$ versus $\delta^{26}Mg_{bulk}$ and $\delta^{26}Mg_{exchangeable}$ in the temperate regolith profile. Green squires represent bedrock, and blue arrows indicate Mg isotope fractionation trends with Mg loss as weathering progresses. Error bars represent 2SD uncertainties.

5.1. Mg Isotope Fractionation in the Temperate Regolith

In the temperate regolith, the low CIA values (49–59, Table S5 in Supporting Information S1) and the preservation of hornblende (Figure 2a) suggest an incipient stage of chemical weathering. The $\tau_{Mg,Th}$ value varies from −7.9% to −51.2% (Table S5 in Supporting Information S1 and Figure 3b), which indicates 7.9%–51.2% Mg loss during chemical weathering. The residual silicate minerals make up more than ∼95% of the total Mg (Table S6 in Supporting Information S1 and Figure 3c), suggesting that residual silicate minerals exert major roles in the δ^{26}Mg values of solid weathering products. In addition, the δ^{26}Mg value is negatively correlated with the $\tau_{Mg,Th}$ value (Figure 5). These results imply that the associated migration and isotope fractionation of Mg are mainly related to residual silicate minerals, including the dissolution of primary minerals and the formation of clay minerals.

It has been recognized that the Mg isotope fractionation caused by primary mineral dissolution can be due to either the preferential release of isotopically light Mg into the fluid (Wimpenny et al., 2010) or the preferential dissolution of isotopically distinct phases (Ma et al., 2015; Ryu et al., 2011). The lack of biotite in the temperate regolith (Figure 2a) suggests preferential dissolution of biotite during chemical weathering. However, given that biotite separates from the bedrock show similar δ^{26}Mg values to bedrock (Table 1), the dissolution of biotite is unlikely to explain the higher δ^{26}Mg in the temperate regolith. The preferential removal of light Mg isotopes due to kinetic effects during the dissolution of primary minerals at the early dissolution stages (within hours or days) was also suggested to fractionate Mg isotopes (Maher et al., 2016; Wimpenny et al., 2010). However, they found that the δ^{26}Mg of the dissolved Mg returned to the value of the initial mineral as the steady-state dissolution rate was approached. Thus, this process is also unlikely to cause the Mg isotope variation in the temperate regolith profile due to the slow rate of chemical weathering.

Alternatively, the variation in Mg isotope composition in this regolith profile is likely caused by the formation of clay minerals. Early kaolinization was observed for K-feldspar and plagioclase in the thin sections under a microscope (Figure S1 in Supporting Information S1), but kaolinite is depleted in Mg (0.03%–0.04% for MgO; Olphen, 1979; Mermut & Cano, 2001) and thus unlikely to have a dominant control on the δ^{26}Mg of the bulk regolith. Confirmation of Mg-bearing clay minerals by XRD was not successful, likely because of a combination of low abundance, low crystallinity, and small size (sub-nanometer). However, the SEM image showed the presence of small number of flake minerals (e.g., illite) (Figure S2 in Supporting Information S1), which have Mg concentrations up to 5.3 wt% based on EDS spot analyses (Table S8 in Supporting Information S1). Therefore, the biotite may weather to clay minerals that are enriched in heavy Mg isotopes (discussed in Section 5.2.1 in detail), resulting in slightly higher δ^{26}Mg values of solid weathering products. This mechanism reconciles well with the lower δ^{26}Mg value in the exchangeable pool when compared to the regolith samples (Figure 4a) since the exchangeable Mg most likely reflects the porewater in which the regolith sample equilibrated (Wimpenny et al., 2014).

5.2. Mg Isotope Fractionation in the Tropical Regolith

In contrast to the temperate regoliths, the tropical regoliths suffered from extreme weathering (CIA > 88). The significantly low $\tau_{Mg,Ta}$ values (−98.5% to −91.4%; Table S5 in Supporting Information S1 and Figure 3b) suggest that most Mg in this profile has been removed. Isotopically heavy Mg is either enriched in the deep regolith (below −250 cm) or depleted in the shallow regolith (above −250 cm) (Figure 4b). Here, we summarize three possible processes contributing to δ^{26}Mg variations in the regolith, including clay mineral formation, atmospheric addition, and plant cycling.

5.2.1. Clay Formation Controls Mg Isotope Composition in Deep Regolith

Magnesium ions in secondary minerals can be adsorbed on a mineral's surface/interlayer (i.e., exchangeable Mg), or tightly bound with oxygen in the crystal structure as impurities (i.e., structural Mg) (e.g., Drever, 1988). It

21699011, 2023, 10, Downloaded from https://agupubs.onlinelibrary.wiley.com/doi/10.1029/2023JF007217 by CAS - Chengdu Library, Wiley Online Library on [16/04/2024]. See the Terms and Conditions (https://onlinelibrary.wiley.com/terms-and-conditions) on Wiley Online Library for rules of use; OA articles are governed by the applicable Creative Commons License

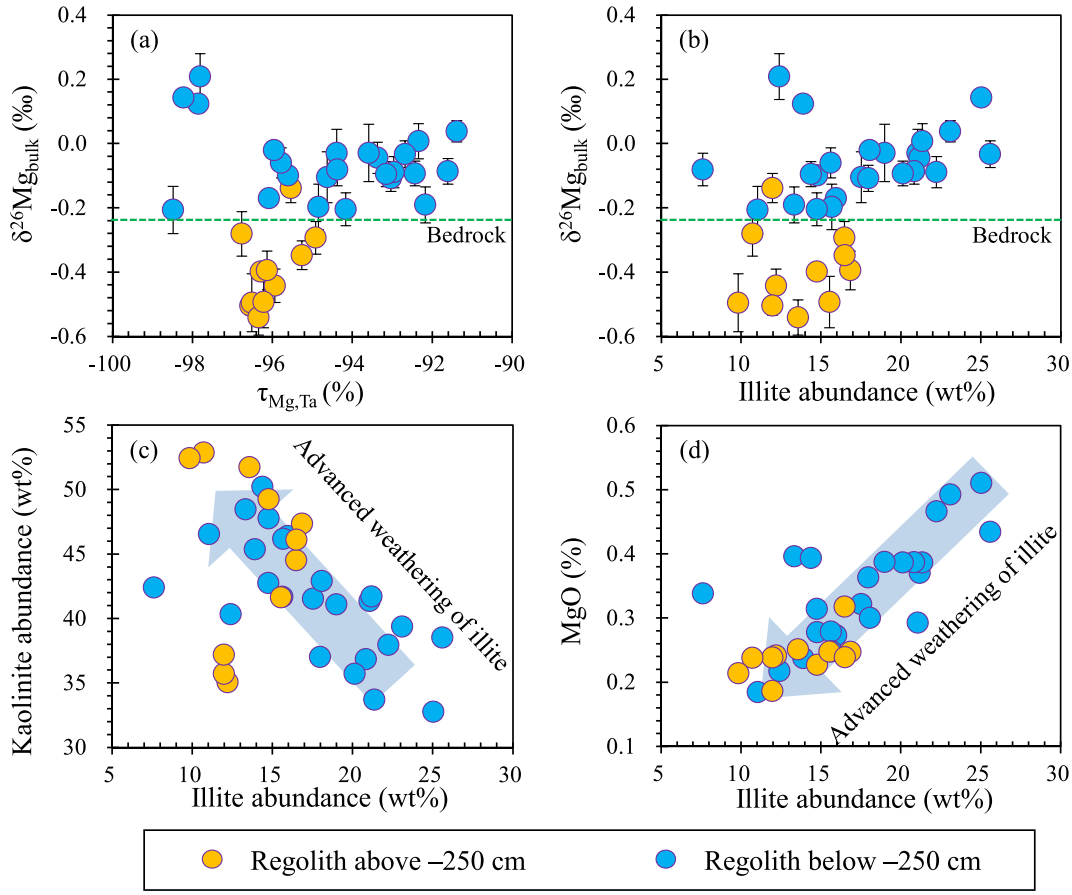

Figure 6. $\tau_{Mg,Ta}$ (a) and illite content (b) versus $\delta^{26}Mg_{bulk}$, and illite content versus kaolinite content (c) and MgO content (d) in the tropical regolith profile. In plots (c, d), blue arrows indicate advanced weathering of illite. Error bars represent 2SD uncertainties.

has been suggested that, in most cases, isotopically heavy Mg is preferentially incorporated into the structural sites of secondary minerals, including clay minerals (e.g., Cai et al., 2022; Wimpenny et al., 2014), crystalline Fe/Al-oxides (e.g., Chapela Lara et al., 2017; Liu et al., 2014), and amorphous minerals (Ryu et al., 2021), whereas the adsorption of exchangeable Mg onto these minerals leads to little or no fractionation of Mg isotopes (Cai et al., 2022; Wimpenny et al., 2014). Our extraction experiments show that more than 96% of Mg sits in the structural sites of residual silicate minerals (Table S6 in Supporting Information S1), most likely in illite because the Mg in amorphous minerals and crystalline Fe oxides only accounts for less than ~4% of the total Mg (Table S6 in Supporting Information S1). This can be understood because illite is an Mg-bearing clay mineral and typically contains high concentrations of structural Mg (2%–3% for MgO; Olphen, 1979). The Mg in illite, like in biotite, is primarily structural, while that in Mg-depleted clay minerals such as kaolinite is primarily adsorbed on surface and interlayer sites (Drever, 1988). The formation of illite thus results in the enrichment of heavy Mg isotopes in the regolith samples below −250 cm (Figures 6a and 6b). This is consistent with the finding by Brewer et al. (2018), who suggested that in situ illite production can lead to a heavy isotopic signature in solid weathering products during granite weathering.

5.2.2. Atmospheric Deposition Controls Mg Isotope Composition in Shallow Regolith

Interestingly, the shallow regoliths (above −250 cm) have $\delta^{26}Mg$ values lower than their bedrock (Figure 4b). In addition, the $\delta^{26}Mg$ value of bulk regolith in the entire profile shows a decreasing trend from the bottom to the top. These results cannot be explained by the above-mentioned primary mineral dissolution and secondary mineral formation processes, as these processes are thought to cause higher $\delta^{26}Mg$ values than bedrock values (e.g., Teng, Li, Rudnick, & Gardner, 2010; Tipper et al., 2012). The illite content was negatively correlated with the kaolinite content but positively correlated with the MgO content (Figures 6c and 6d), indicating the

21699011, 2023, 10, Downloaded from https://agupubs.onlinelibrary.wiley.com/doi/10.1029/2023JF007217 by CAS - Chengdu Library, Wiley Online Library on [16/04/2024]. See the Terms and Conditions (https://onlinelibrary.wiley.com/terms-and-conditions) on Wiley Online Library for rules of use; OA articles are governed by the applicable Creative Commons License

21699011, 2023, 10, Downloaded from https://agupubs.onlinelibrary.wiley.com/doi/10.1029/2023JF007217 by CAS - Chengdu Library, Wiley Online Library on [16/04/2024]. See the Terms and Conditions (https://onlinelibrary.wiley.com/terms-and-conditions) on Wiley Online Library for rules of use; OA articles are governed by the applicable Creative Commons License

progressive weathering of illite. However, this process alone cannot explain the δ^{26}Mg data because most Mg is present in structural sites of illite; thus, the regolith samples would remain unchanged even if some illites have been weathered. Another possible explanation is the successive adsorption-desorption of heavy Mg isotopes (Huang et al., 2012; Opfergelt et al., 2014), but this process seems unlikely because of the small amount of exchangeable Mg in the samples (Figure 3d). In addition, recent batch experiments have demonstrated negligible Mg isotope fractionation during adsorption-desorption processes (Cai et al., 2022). Carbonate minerals are known to have the most negative δ^{26}Mg values in environmental samples (Saenger & Wang, 2014), but microscopic and XRD analyses failed to identify the presence of carbonate minerals. This is also evidenced by the small amount of Mg leached by 0.5 mol L^{-1} HCl (<2%; Table S6 in Supporting Information S1).

We ascribe the low δ^{26}Mg values in the shallow regolith to atmospheric addition. In the following discussion, we consider two potential atmospheric sources in the study area: aeolian dust and rainwater and/or marine aerosols. The aeolian dust deposition has been suggested to lower the δ^{26}Mg values in the near surface samples (Liu et al., 2014). Likewise, the deposition of loess soured from North China may also influence the δ^{26}Mg values in the shallow regolith samples, as the site is located close to the most important aeolian dust sources in Asia. Variations in radiogenic Nd isotope ratios have been used to determine aeolian inputs and their sources (e.g., Liu et al., 2013; Pett-Ridge et al., 2009). Our results show that the ε_{Nd} values in the shallow regolith (−16.51 to −14.54) are markedly lower than those in the aeolian dust since ∼52 Ma (−12 to −8; Yang et al., 2021) (Figure S3 in Supporting Information S1), confirming the limited dust contribution.

Alternatively, the enrichment of isotopically light Mg in the shallow regolith is most likely due to the deposition of rainwater and/or marine aerosols, which has also been observed in previous studies (Opfergelt et al., 2012, 2014). The shallow regolith in near-coastal settings (approximately 70 km from the sea; Figure 1) is susceptible to the deposition of marine aerosols and rainwater. As an extreme chemical weathering in a humid climate with low evapotranspiration over precipitation (mean precipitation ∼1,691 mm yr^{-1}) removes most Mg from granite ($\tau_{Mg,Ta}$ < −87%; Figure 3b), atmospheric Mg from marine aerosols (−0.83 ± 0.09‰, 2SD, n = 90; Ling et al., 2011) and rainwater (−1.13 ± 0.75‰, 2SD, n = 7; Cai et al., 2022; T. Gao et al., 2018; Tipper et al., 2012) can contribute a significant amount of isotopically light Mg to the soil solution and/or soil exchange complex (Opfergelt et al., 2014). The Mg from rainwater and/or marine aerosols may deposit on the surface of soil. Some may even move deeper into the profile and enter the crystal structure of the illite during its formation. The deposited Mg can overprint the granitic Mg, and the δ^{26}Mg value of regolith samples will reflect mixing between granitic and aerosol/rainwater sources.

5.2.3. Plant Cycling

Magnesium is an essential nutrient for plant growth (Montezano et al., 2013; Wilkinson et al., 1990), and the life cycle of plants is accompanied by the cycling of Mg in soil systems. The plant-available Mg ions (exchangeable and dissolved Mg) in soils are taken up by roots and stored in plants for several months or years, and then released back into soils via secretion and decay. These biological processes could potentially modify the δ^{26}Mg values of shallow regolith samples in the following way (e.g., Bolou-Bi et al., 2012; Uhlig et al., 2017). First, plants have been shown to preferentially take up ^{26}Mg (Bolou-Bi et al., 2010), leaving ^{24}Mg enriched in the soil solution and an exchangeable pool close to the root. Second, the Mg returned from plants shifts the surface soil to either higher or lower δ^{26}Mg values (e.g., T. Gao et al., 2018; Uhlig et al., 2017).

Although such a mechanism is plausible to affect Mg isotope variations in top-soils, it may only play a minor role because of the very small amount of TOC content measured (<0.4 wt%; Table S5 in Supporting Information S1). The increased δ^{26}Mg values with decreasing depth in the regolith samples above −90 cm (Figure 4b) are likely attributed to the illite formation rather than biological cycling; both TOC and illite content show positive correlations with δ^{26}Mg values (Figure S4 in Supporting Information S1). However, biological cycling may influence the Mg isotope composition of the exchangeable Mg pool. As observed in the regolith samples above −90 cm, the δ^{26}Mg value of the exchangeable Mg pool decreases from the bottom to the top (Figure 4b), which is potentially caused by the preferential uptake of isotopically heavy Mg from the exchangeable pool.

5.3. Implications

Continental weathering releases Mg from silicates into rivers, which eventually enter the ocean (Tipper et al., 2006). Therefore, understanding Mg isotope behavior during continental weathering is critical in determining riverine

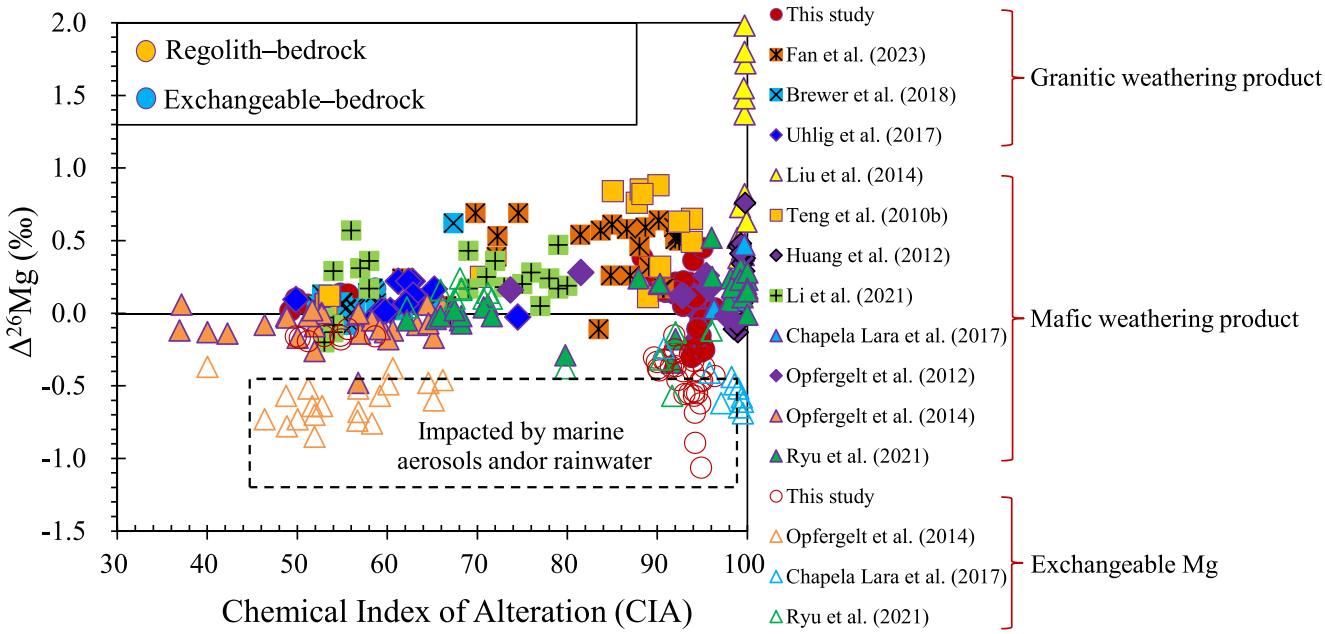

Figure 7. Chemical Index of Alteration (CIA) versus the difference ($\Delta^{26}Mg$) in $\delta^{26}Mg$ between the bedrock and regolith and between the bedrock and exchangeable pool. Mg isotope ratios are from this study and the literature (Brewer et al., 2018; Chapela Lara et al., 2017; Fan et al., 2023; Huang et al., 2012; Li et al., 2021; Liu et al., 2014; Opfergelt et al., 2012, 2014; Ryu et al., 2021; Teng, Li, Rudnick, & Gardner, 2010; Tipper et al., 2012; Uhlig et al., 2017).

input to the oceans (Tipper et al., 2006). Comparing our results with published data of regolith profiles developed on silicate rocks (including basalts, andesites, and granites) on the $\delta^{26}Mg$ versus CIA plot (Brewer et al., 2018; Chapela Lara et al., 2017; Fan et al., 2023; Huang et al., 2012; Li et al., 2021; Liu et al., 2014; Opfergelt et al., 2012, 2014; Ryu et al., 2021; Teng, Li, Rudnick, & Gardner, 2010; Tipper et al., 2012; Uhlig et al., 2017; Figure 7), it can be noted that the major control on the difference in Mg isotope composition ($\Delta^{26}Mg_{regolith\text{-}bedrock}$) between regolith and bedrock is the weathering intensity, that is, as CIA increases or chemical weathering intensifies, $\Delta^{26}Mg_{regolith\text{-}bedrock}$ increases as a result of the formation of secondary clay minerals, as suggested by many previous studies (e.g., Liu et al., 2014; Opfergelt et al., 2012; Teng, Li, Rudnick, & Gardner, 2010). For example, the CIA values of regolith samples in our BJ profile are significantly lower than those in the deep section of our GD profile, and $\Delta^{26}Mg_{regolith\text{-}bedrock}$ values in our BJ profile are much lower than those in the deep section of our GD profile. Besides this general trend, Figure 7 also shows some intricate complexities in $\Delta^{26}Mg_{regolith\text{-}bedrock}$ variations, likely caused by factors including rock types, climatic parameters, and even atmospheric depositions.

One major difference between granite and basalt weathering is that granite often tends to weather slower than basalt (e.g., Bluth & Kump, 1994; Hayes et al., 2020; Oliva et al., 2003) and shows smaller CIA and $\Delta^{26}Mg_{regolith\text{-}bedrock}$ values (e.g., in our BJ regolith profile). Moreover, the formation of secondary minerals preferentially holds isotopically heavy Mg in regolith (Wimpenny et al., 2014), and thus, the regolith, in general, has $\delta^{26}Mg$ values much higher than those of the bedrock (e.g., Opfergelt et al., 2012; Teng, Li, Rudnick, & Gardner, 2010). Accordingly, the dissolved Mg may have lower $\delta^{26}Mg$ values than those with only dissolution of primary minerals. However, under extreme weathering conditions, because granite regolith samples typically contain low concentrations of Mg, the shallow section of granite regolith is subject to the influence of atmospheric deposition, as shown in our GD profile and the andesite weathering profile reported by Opfergelt et al. (2012). The riverine $\delta^{26}Mg$ value may therefore reflect a combination of atmospheric inputs and weathering processes.

The difference in the weathering intensity (as reflected in CIA values) between our BJ and GD weathering profiles is likely influenced by climatic parameters. The temperate climate with low precipitation and vegetation coverage in the BJ section likely results in a slower weathering rate (and thus less Mg isotope fractionation), while the tropical humid climate with high precipitation and warm temperature will cause a fast weathering rate and intensive weathering in the GD section. These results imply that the riverine $\delta^{26}Mg$ value may be affected not only by rock type in the drainage basin but also by climatic factors. More similar studies in different weathering regimes (especially at the moderate weathering stage) are needed to decipher the relative importance of other

21699011, 2023, 10, Downloaded from https://agupubs.onlinelibrary.wiley.com/doi/10.1029/2023JF007217 by CAS - Chengdu Library, Wiley Online Library on [16/04/2024]. See the Terms and Conditions (https://onlinelibrary.wiley.com/terms-and-conditions) on Wiley Online Library for rules of use; OA articles are governed by the applicable Creative Commons License

21699011, 2023, 10, Downloaded from https://agupubs.onlinelibrary.wiley.com/doi/10.1029/2023JF007217 by CAS - Chengdu Library, Wiley Online Library on [16/04/2024]. See the Terms and Conditions (https://onlinelibrary.wiley.com/terms-and-conditions) on Wiley Online Library for rules of use; OA articles are governed by the applicable Creative Commons License

factors (including the type of vegetation cover, age of soil development, and erosion history) on Mg isotope variations during silicate weathering.

6. Conclusions

This study presents the mineralogy, element concentrations, and Mg isotope compositions of bulk and exchangeable fractions in two granite regolith profiles from China developed under temperate, semiarid and tropical, humid climate conditions. The following conclusions can be drawn from our results and discussions.

1. The slightly higher δ^{26}Mg value in the bulk regolith and visibly lower δ^{26}Mg value in the exchangeable pool in the temperate regolith profile than in the bedrock may be caused by the formation of small number of clay minerals at the initial chemical weathering stage.
2. The large variation in the δ^{26}Mg value of the bulk regolith and exchangeable fraction results from the mixing of Mg from solid weathering products and atmospheric inputs (marine aerosols and/or rainwater). The formation of illite preferentially takes up isotopically heavy Mg into its crystal structures. However, the input of atmospheric Mg contributes light Mg isotopes that may enter the illite structure and dominates the δ^{26}Mg values of the bulk regolith, which has very low Mg content due to extreme weathering.
3. Our study demonstrated that climate may have a significant impact on Mg isotope fractionation during terrestrial weathering, which is of significance to interpret the Mg isotope compositions of weathering products and river waters at a global scale.

Conflict of Interest

The authors declare no conflicts of interest relevant to this study.

Data Availability Statement

All data used in this study are stored in the Research Data Repository of Mendeley data (Gao et al., 2023), and can be accessed at https://data.mendeley.com/datasets/bh62p4rtr2/1.

Acknowledgments
We thank Hairuo Mao for his comments on the manuscript. We also thank Dehan Shen for the help when conducting the SEM experiment. This work was funded by the Strategic Priority Research Program of The Chinese Academy of Sciences (XDB40020400) and the China Postdoctoral Science Foundation (2020M683377).

References

Berner, R. A., Lasaga, A. C., & Garrels, R. M. (1983). The carbonate-silicate geochemical cycle and its effect on atmospheric carbon dioxide over the past 100 million years. *American Journal of Science*, *57*(7), 641–683. https://doi.org/10.2475/ajs.283.7.641

Bluth, G. J., & Kump, L. R. (1994). Lithologic and climatologic controls of river chemistry. *Geochimica et Cosmochimica Acta*, *58*(10), 2341–2359. https://doi.org/10.1016/0016-7037(94)90015-9

Bolou-Bi, E. B., Poszwa, A., Leyval, C., & Vigier, N. (2010). Experimental determination of magnesium isotope fractionation during higher plant growth. *Geochimica et Cosmochimica Acta*, *74*(9), 2523–2537. https://doi.org/10.1016/j.gca.2010.02.010

Bolou-Bi, E. B., Vigier, N., Poszwa, A., Boudot, J.-P., & Dambrine, E. (2012). Effects of bio-geochemical processes on magnesium isotope variations in a forested catchment in the Vosges Mountains (France). *Geochimica et Cosmochimica Acta*, *87*, 341–355. https://doi.org/10.1016/j.gca.2012.04.005

Brady, P. V. (1991). The effect of silicate weathering on global temperature and atmospheric CO_2. *Journal of Geophysical Research*, *96*(B11), 18101–18106. https://doi.org/10.1029/91jb01898

Braun, J. J., Pagel, M., Herbillon, A., & Rosin, C. (1993). Mobilization and redistribution of rees and thorium in a syenitic lateritic profile—A mass-balance study. *Geochimica et Cosmochimica Acta*, *57*(18), 4419–4434. https://doi.org/10.1016/0016-7037(93)90492-f

Brenot, A., Cloquet, C., Vigier, N., Carignan, J., & France-Lanord, C. (2008). Magnesium isotope systematics of the lithologically varied Moselle river basin, France. *Geochimica et Cosmochimica Acta*, *72*(20), 5070–5089. https://doi.org/10.1016/j.gca.2008.07.027

Brewer, A., Teng, F.-Z., & Dethier, D. (2018). Magnesium isotope fractionation during granite weathering. *Chemical Geology*, *501*, 95–103. https://doi.org/10.1016/j.chemgeo.2018.10.013

Brimhall, G. H., & Dietrich, W. E. (1987). Constitutive mass balance relations between chemical composition, volume, density, porosity, and strain in metasomatic hydrochemical systems: Results on weathering and pedogenesis. *Geochimica et Cosmochimica Acta*, *51*(3), 567–587. https://doi.org/10.1016/0016-7037(87)90070-6

Cai, D., Henehan, M. J., Uhlig, D., & von Blanckenburg, F. (2022). Mg isotope composition of runoff is buffered by the regolith exchangeable pool. *Geochimica et Cosmochimica Acta*, *321*, 99–114. https://doi.org/10.1016/j.gca.2022.01.011

Cai, J.-H., Yan, G.-H., Mu, B.-L., Reng, K.-X., Song, B., & Li, F.-T. (2005). Zircon U-Pb age, Sr-Nd-Pb isotopic compositions and trace element of Fangshan complex in Beijing and their petrogenesis significance. *Acta Petrologica Sinica*, *21*, 776–788.

Chapela Lara, M., Buss, H. L., Pogge von Strandmann, P. A. E., Schuessler, J. A., & Moore, O. W. (2017). The influence of critical zone processes on the Mg isotope bud-get in a tropical, highly weathered andesitic catchment. *Geochimica et Cosmochimica Acta*, *202*, 77–100. https://doi.org/10.1016/j.gca.2016.12.032

Colla, C. A., Casey, W. H., & Ohlin, C. A. (2018). Computational prediction of Mg-isotope fractionation between aqueous $[Mg(OH_2)_6]^{2+}$ and brucite. *Geochimica et Cosmochimica Acta*, *227*, 64–74. https://doi.org/10.1016/j.gca.2018.02.005

Dessert, C., Dupre, B., Gaillardet, J., Francois, L. M., & Allegre, C. J. (2003). Basalt weathering laws and the impact of basalt weathering on the global carbon cycle. *Chemical Geology*, *202*(3–4), 257–273. https://doi.org/10.1016/j.chemgeo.2002.10.001

Drever, J. I. (1988). *The Geochemistry of natural waters*. Prentice Hall.
Fan, B., Yang, X. Q., Jiang, K., & Zhao, Z. Q. (2023). Processes controlling the Mg isotope behavior during granite weathering. *Journal of Asian Earth Sciences*, *251*, 105674. https://doi.org/10.1016/j.jseaes.2023.105674
Gaillardet, J., Dupré, B., Louvat, P., & Allegre, C. J. (1999). Global silicate weathering and CO_2 consumption rates deduced from the chemistry of large rivers. *Chemical Geology*, *159*(1–4), 3–30. https://doi.org/10.1016/s0009-2541(99)00031-5
Gao, C., Cao, X., Liu, Q., Yang, Y., Zhang, S., He, Y., et al. (2018). Theoretical calculation of equilibrium Mg isotope fractionations between minerals and aqueous solutions. *Chemical Geology*, *488*, 62–75. https://doi.org/10.1016/j.chemgeo.2018.04.005
Gao, T., Ke, S., Li, R., Meng, X.-N., He, Y., Liu, C., et al. (2019). High-precision magnesium isotope analysis of geological and environmental reference materials by multiple-collector inductively coupled plasma mass spectrometry. *Rapid Communications in Mass Spectrometry*, *33*(8), 767–777. https://doi.org/10.1002/rcm.8376
Gao, T., Ke, S., Wang, S.-J., Li, F., Liu, C., Lei, J., et al. (2018). Contrasting Mg isotopic compositions between Fe-Mn nodules and surrounding soils: Accumulation of light Mg isotopes by Mg-depleted clay minerals and Fe oxides. *Geochimica et Cosmochimica Acta*, *237*, 205–222. https://doi.org/10.1016/j.gca.2018.06.028
Gao, T., Qi, M., Wang, Z. R., Yin, R. S., Liu, C. S., Liu, Y. H., et al. (2023). Contrasting Mg isotope compositions in temperate and tropical regoliths: Possible implications for climate control (Version 1) [Dataset]. Mendeley Data. https://data.mendeley.com/datasets/bh62p4rtr2/1
Graulis, S., Chateigner, D., Downs, R. T., Yokochi, A. F. T., Bail, A. L., Lutterotti, L., et al. (2009). Crystallography open database—An open-access collection of crystal structures. *Journal of Applied Crystallography*, *42*(4), 726–729. https://doi.org/10.1107/s0021889809016690
Hayes, N. R., Buss, H. L., Moore, O. W., Krám, P., & Pancost, R. D. (2020). Controls on granitic weathering fronts in contrasting climates. *Chemical Geology*, *535*, 119450. https://doi.org/10.1016/j.chemgeo.2019.119450
Hindshaw, R. S., Rebecca, T., Nicholas, J. T., & Tipper, E. T. (2020). Experimental constraints on Mg isotope fractionation during clay formation: Implications for the global biogeochemical cycle of Mg. *Earth and Planetary Science Letters*, *531*, 115980. https://doi.org/10.1016/j.epsl.2019.115980
Huang, K.-J., Teng, F.-Z., Wei, G.-J., Ma, J.-L., & Bao, Z.-Y. (2012). Adsorption- and desorption-controlled magnesium isotope fractionation during extreme weathering of basalt in Hainan Island, China. *Earth and Planetary Science Letters*, *359*, 73–83. https://doi.org/10.1016/j.epsl.2012.10.007
Jacobson, A. D., Zhang, Z., Lundstrom, C., & Huang, F. (2010). Behavior of Mg isotopes during dedolomitization in the Madison Aquifer, South Dakota. *Earth and Planetary Science Letters*, *297*(3–4), 446–452. https://doi.org/10.1016/j.epsl.2010.06.038
Jweda, J., Bolge, L., Class, C., & Goldstein, S. L. (2016). High precision Sr-Nd-Hf-Pb isotopic compositions of USGS reference material BCR-2. *Geostandards and Geoanalytical Research*, *40*(1), 101–115. https://doi.org/10.1111/j.1751-908x.2015.00342.x
Kurtz, A. C., Derry, L. A., Chadwick, O. A., & Alfano, M. J. (2000). Refractory element mobility in volcanic soils. *Geology*, *28*(8), 683–686. https://doi.org/10.1130/0091-7613(2000)28<683:remivs>2.0.co;2
Li, M. Y. H., Teng, F.-Z., & Zhou, M.-F. (2021). Phyllosilicate controls on magnesium isotopic fractionation during weathering of granites: Implications for continental weathering and riverine system. *Earth and Planetary Science Letters*, *553*, 116613. https://doi.org/10.1016/j.epsl.2020.116613
Li, W., Beard, B. L., Li, C., & Johnson, C. M. (2014). Magnesium isotope fractionation between brucite [$Mg(OH)_2$] and Mg aqueous species: Implications for silicate weathering and biogeochemical processes. *Earth and Planetary Science Letters*, *394*, 82–93. https://doi.org/10.1016/j.epsl.2014.03.022
Li, X., Li, W., & Li, Z.-X. (2007). On the genetic classification and tectonic implications of the Early Yanshanian granitoids in the Nanling Range, South China. *Chinese Science Bulletin*, *52*(14), 1873–1885. https://doi.org/10.1007/s11434-007-0259-0
Ling, M.-X., Sedaghatpour, F., Teng, F.-Z., Hays, P. D., Strauss, J., & Sun, W. (2011). Homogenous magnesium isotopic composition of seawater: An excellent geostandard for Mg isotope analysis. *Rapid Communications in Mass Spectrometry*, *25*(19), 2828–2836. https://doi.org/10.1002/rcm.5172
Liu, X.-M., Teng, F.-Z., Rudnick, R. L., McDonough, W. F., & Cummings, M. L. (2014). Massive magnesium depletion and isotope fractionation in weathered basalts. *Geochimica et Cosmochimica Acta*, *135*, 336–349. https://doi.org/10.1016/j.gca.2014.03.028
Liu, X. M., Rudnick, R. L., Mcdonough, W. F., & Cummings, M. (2013). Influence of chemical weathering on the composition of the continental crust: Insights from Li and Nd isotopes in bauxite profiles developed on Columbia river basalts. *Geochimica et Cosmochimica Acta*, *115*, 73–91. https://doi.org/10.1016/j.gca.2013.03.043
Ma, L., Teng, F. Z., Jin, L., Ke, S., Yang, W., Gu, H. O., & Brantley, S. L. (2015). Magnesium isotope fractionation during shale weathering in the Shale Hills Critical Zone Observatory: Accumulation of light Mg isotopes in soils by clay mineral transformation. *Chemical Geology*, *397*, 37–50. https://doi.org/10.1016/j.chemgeo.2015.01.010
Maher, K., Johnson, N. C., Jackson, A., Lammers, L. N., Torchinsky, A. B., Weaver, K. L., et al. (2016). A spatially resolved surface kinetic model for forsterite dissolution. *Geochimica et Cosmochimica Acta*, *174*, 313–334. https://doi.org/10.1016/j.gca.2015.11.019
Mermut, A. R., & Cano, A. F. (2001). Baseline studies of the clay minerals society source clays: Chemical analyses of major elements. *Clays and Clay Minerals*, *49*(5), 381–386. https://doi.org/10.1346/ccmn.2001.0490504
Montezano, A. C., Antunes, T. T., Callera, G., & Touyz, R. M. (2013). Magnesium and vessels. In *Encyclopedia of metalloproteins* (pp. 1238–2124). Springer.
Murphy, B. P., Johnson, J. P. L., Gasparini, N. M., & Sklar, L. S. (2016). Chemical weathering as a mechanism for the climatic control of bedrock river incision. *Nature*, *532*(7598), 223–227. https://doi.org/10.1038/nature17449
Nesbitt, H. W., & Markovics, G. (1997). Weathering of granodioritic crust, long-term storage of elements in weathering profiles, and petrogenesis of siliciclastic sediments. *Geochimica et Cosmochimica Acta*, *61*(8), 1653–1670. https://doi.org/10.1016/s0016-7037(97)00031-8
Nesbitt, H. W., & Wilson, R. E. (1992). Recent chemical weathering of basalts. *American Journal of Science*, *292*(10), 740–777. https://doi.org/10.2475/ajs.292.10.740
Nesbitt, H. W., & Young, G. M. (1982). Early Proterozoic climates and plate motions inferred from major element chemistry of lutites. *Nature*, *299*(5885), 715–717. https://doi.org/10.1038/299715a0
Oliva, P., Viers, J., & Dupré, B. (2003). Chemical weathering in granitic environments. *Chemical Geology*, *202*(3–4), 225–256. https://doi.org/10.1016/j.chemgeo.2002.08.001
Olphen, E. H. V. (1979). Data handbook for clay materials and other nonmetallic minerals.
Opfergelt, S., Burton, K. W., Georg, R. B., West, A. J., Guicharnaud, R. A., Sigfusson, B., et al. (2014). Magnesium retention on the soil exchange complex controlling Mg isotope variations in soils, soil solutions and vegetation in volcanic soils Iceland. *Geochimica et Cosmochimica Acta*, *125*, 110–130. https://doi.org/10.1016/j.gca.2013.09.036

21699011, 2023, 10, Downloaded from https://agupubs.onlinelibrary.wiley.com/doi/10.1029/2023JF007217 by CAS - Chengdu Library, Wiley Online Library on [16/04/2024]. See the Terms and Conditions (https://onlinelibrary.wiley.com/terms-and-conditions) on Wiley Online Library for rules of use; OA articles are governed by the applicable Creative Commons License

Opfergelt, S., Georg, R. B., Delvaux, B., Cabidoche, Y. M., Burton, K. W., & Halliday, A. N. (2012). Mechanisms of magnesium isotope fractionation in volcanic soil weathering sequences, Guadeloupe. *Earth and Planetary Science Letters*, *341*, 176–185. https://doi.org/10.1016/j.epsl.2012.06.010

Pett-Ridge, J. C., Derry, L. A., & Kurtz, A. C. (2009). Sr isotopes as a tracer of weathering processes and dust inputs in a tropical granitoid watershed, Luquillo Mountains, Puerto Rico. *Geochimica et Cosmochimica Acta*, *73*(1), 25–43. https://doi.org/10.1016/j.gca.2008.09.032

Pogge von Strandmann, P. A. E., Burton, K. W., James, R. H., van Calsteren, P., Gislason, S. R., & Sigfússon, B. (2008). The influence of weathering processes on riverine magnesium isotopes in a basaltic terrain. *Earth and Planetary Science Letters*, *276*(1–2), 187–197. https://doi.org/10.1016/j.epsl.2008.09.020

Pogge von Strandmann, P. A. E., Opfergelt, S., Lai, Y. J., Sigfússon, B., Gislason, S. R., & Burton, K. W. (2012). Lithium, magnesium and silicon isotope behaviour accompanying weathering in a basaltic soil and pore water regolith in Iceland. *Earth and Planetary Science Letters*, *339*, 11–23. https://doi.org/10.1016/j.epsl.2012.05.035

Raczek, I., Jochum, K. P., & Hofmann, A. W. (2003). Neodymium and strontium isotope data for USGS reference materials BCR-1, BCR-2, BHVO-1, BHVO-2, AGV-1, AGV-2, GSP-1, GSP-2 and eight MPI-DING reference glasses. *Geostandards Newsletter*, *27*(2), 173–179. https://doi.org/10.1111/j.1751-908x.2003.tb00644.x

Ryu, J.-S., Jacobson, A. D., Holmden, C., Lundstrom, C., & Zhang, Z.-F. (2011). The major ion, $\delta^{44/40}$Ca, $\delta^{44/42}$Ca, and $\delta^{26/24}$Mg geochemistry of granite weathering at pH=1 and T=25°C: Power-law processes and the relative reactivity of minerals. *Geochimica et Cosmochimica Acta*, *75*(20), 6004–6026. https://doi.org/10.1016/j.gca.2011.07.025

Ryu, J.-S., Vigier, N., Decarreau, A., Lee, S.-W., Lee, K.-S., Song, H., & Petit, S. (2016). Experimental investigation of Mg isotope fractionation during mineral dissolution and clay formation. *Chemical Geology*, *445*, 135–145. https://doi.org/10.1016/j.chemgeo.2016.02.006

Ryu, J.-S., Vigier, N., Derry, L., & Chadwick, O. A. (2021). Variations of Mg isotope geochemistry in soils over a Hawaiian 4 Myr chronosequence. *Geochimica et Cosmochimica Acta*, *292*, 94–114. https://doi.org/10.1016/j.gca.2020.09.024

Saenger, C., & Wang, Z. (2014). Magnesium isotope fractionation in biogenic and abiogenic carbonates: Implications for pale-oenvironmental proxies. *Quaternary Science Reviews*, *90*, 1–21. https://doi.org/10.1016/j.quascirev.2014.01.014

Schuessler, J. A., von Blanckenburg, F., Bouchez, J., Uhlig, D., & Hewawasam, T. (2018). Nutrient cycling in a tropical montane rainforest under a supply-limited weathering regime traced by elemental mass balances and Mg stable isotopes. *Chemical Geology*, *497*, 74–87. https://doi.org/10.1016/j.chemgeo.2018.08.024

Tanaka, T., Togashi, S., Kamioka, H., Amakawa, H., Kagami, H., Hamamoto, T., et al. (2000). JNdi-1: A neodymium isotopic reference in consistency with LaJolla neodymium. *Chemical Geology*, *168*(3–4), 279–281. https://doi.org/10.1016/s0009-2541(00)00198-4

Teng, F.-Z., Li, W.-Y., Ke, S., Marty, B., Dauphas, N., Huang, S., et al. (2010). Magnesium isotopic composition of the Earth and chondrites. *Geochimica et Cosmochimica Acta*, *74*(14), 4150–4166. https://doi.org/10.1016/j.gca.2010.04.019

Teng, F.-Z., Li, W.-Y., Ke, S., Yang, W., Liu, S.-A., Sedaghatpour, F., et al. (2015). Magnesium isotopic compositions of international geological reference materials. *Geostandards and Geoanalytical Research*, *39*(3), 329–339. https://doi.org/10.1111/j.1751-908x.2014.00326.x

Teng, F.-Z., Li, W.-Y., Rudnick, R. L., & Gardner, L. R. (2010). Contrasting lithium and magnesium isotope fractionation during continental weathering. *Earth and Planetary Science Letters*, *300*(1–2), 63–71. https://doi.org/10.1016/j.epsl.2010.09.036

Tipper, E. T., Gaillardet, J., Louvat, P., Capmas, F., & White, A. F. (2010). Mg isotope constraints on soil pore-fluid chemistry: Evidence from Santa Cruz, California. *Geochimica et Cosmochimica Acta*, *74*(14), 3883–3896. https://doi.org/10.1016/j.gca.2010.04.021

Tipper, E. T., Galy, A., & Bickle, M. J. (2008). Calcium and magnesium isotope systematics in rivers draining the Himalaya-Tibetan-Plateau region: Lithological or fractiona-tion control? *Geochimica et Cosmochimica Acta*, *72*(4), 1057–1075. https://doi.org/10.1016/j.gca.2007.11.029

Tipper, E. T., Galy, A., Gaillardet, J., Bickle, M. J., Elderfield, H., & Carder, E. A. (2006). The magnesium isotope budget of the modern ocean: Constraints from riverine magnesium isotope ratios. *Earth and Planetary Science Letters*, *250*(1–2), 241–253. https://doi.org/10.1016/j.epsl.2006.07.037

Tipper, E. T., Lemarchand, E., Hindshaw, R. S., Reynolds, B. C., & Bourdon, B. (2012). Seasonal sensitivity of weathering processes: Hints from magnesium isotopes in a glacial stream. *Chemical Geology*, *312*, 80–92. https://doi.org/10.1016/j.chemgeo.2012.04.002

Uhlig, D., Schuessler, J. A., Bouchez, J., Dixon, J. L., & von Blanckenburg, F. (2017). Quantifying nutrient uptake as driver of rock weathering in forest ecosystems by magnesium stable isotopes. *Biogeosciences*, *14*(12), 3111–3128. https://doi.org/10.5194/bg-14-3111-2017

Volk, T. (1987). Feedbacks between weathering and atmospheric CO_2 over the last 100 million years. *American Journal of Science*, *287*(8), 763–779. https://doi.org/10.2475/ajs.287.8.763

Wang, W., Zhou, C., Liu, Y., Wu, Z., & Huang, F. (2019). Equilibrium Mg isotope fractionation among aqueous Mg^{2+}, carbonates, brucite and lizardite: Insights from firstprinciples molecular dynamics simulations. *Geochimica et Cosmochimica Acta*, *250*, 117–129. https://doi.org/10.1016/j.gca.2019.01.042

Wei, X., Shi, X. F., Xu, Y. G., Castillo, P. R., Zhang, Y., Zhang, L., & Zhang, H. (2022). Mid-Cretaceous Wake seamounts in NW Pacific originate from secondary mantle plumes with Arago hotspot composition. *Chemical Geology*, *587*, 120632. https://doi.org/10.1016/j.chemgeo.2021.120632

Wiederhold, J. G., Teutsch, N., Kraemer, S. M., Halliday, A. N., & Kretzschmar, R. (2007). Iron isotope fractionation in oxic soils by mineral weathering and podzolization. *Geochimica et Cosmochimica Acta*, *71*(23), 5821–5833. https://doi.org/10.1016/j.gca.2007.07.023

Wilkinson, S., Welch, R., Mayland, H., & Grunes, D. (1990). Magnesium in plants: Uptake, distribution, function and utilization by man and animals. *Metal Ions in Biological Systems*, *26*, 33–56.

Wimpenny, J., Burton, K. W., James, R. H., Gannoun, A., Mokadem, F., & Gíslason, S. R. (2011). The behaviour of magnesium and its isotopes during glacial weathering in an ancient shield terrain in West Greenland. *Earth and Planetary Science Letters*, *304*(1–2), 260–269. https://doi.org/10.1016/j.epsl.2011.02.008

Wimpenny, J., Colla, C. A., Yin, Q.-Z., Rustad, J. R., & Casey, W. H. (2014). Investigating the behaviour of Mg isotopes during the formation of clay minerals. *Geochimica et Cosmochimica Acta*, *128*, 178–194. https://doi.org/10.1016/j.gca.2013.12.012

Wimpenny, J., Gíslason, S. R., James, R. H., Gannoun, A., Pogge von Strandmann, P. A. E., & Burton, K. W. (2010). The behaviour of Li and Mg isotopes during primary phase dissolution and secondary mineral formation in basalt. *Geochimica et Cosmochimica Acta*, *74*(18), 5259–5279. https://doi.org/10.1016/j.gca.2010.06.028

Yang, Y., Galy, A., Fang, X., Yang, R., Zhang, W., Song, B., et al. (2021). Neodymium isotopic constraints on Cenozoic Asian dust provenance changes linked to the exhumation history of the northern Tibetan Plateau and the Central Asian Orogenic Belt. *Geochimica et Cosmochimica Acta*, *296*, 38–55. https://doi.org/10.1016/j.gca.2020.12.026

Young, R. A. (1993). *The rietveld method. International union of crystallography monographs on crystallography*. Oxford University Press.

Young, E. D., & Galy, A. (2004). The isotope geochemistry and cosmochemistry of magnesium. *Reviews in Mineralogy and Geochemistry*, *55*, 197–230. https://doi.org/10.2138/gsrmg.55.1.197

21699011, 2023, 10, Downloaded from https://agupubs.onlinelibrary.wiley.com/doi/10.1029/2023JF007217 by CAS - Chengdu Library, Wiley Online Library on [16/04/2024]. See the Terms and Conditions (https://onlinelibrary.wiley.com/terms-and-conditions) on Wiley Online Library for rules of use; OA articles are governed by the applicable Creative Commons License